Simulating Heavy Ion SEUs in the ESA Monitor

Author:
Emil Noordeh

Supervisor:
Rubén Garcia Alia

IPP CERN Summer Student Project

Radiation to Electronics Department (R2E)
CERN: EN-STI-EET

October 2014

Abstract

Radiation to Electronics Department (R2E)

CERN: EN-STI-EET

Simulating Heavy Ion SEUs in the ESA Monitor

by Emil Noordeh

This study analyzed SEU measurements made of the ESA Monitor at GSI, RADEF, UCL, and TAMU. An IRPP model was implemented through the use of FLUKA that was calibrated to the measurements of ions above the LET threshold. The model proved successful in reproducing proton measurements that are entirely independent of the calibration. When applied to the sub-threshold region, experimental measurements were underestimated by a factor of ∼3 for the high energy ions at GSI, a factor of ∼10 for the ions at UCL/RADEF, and an anomalous factor of ∼300 for the ion at TAMU. Several possible sources of systematic uncertainty were investigated including sensitive volume size, BEOL thickness, and substrate thickness. Additionally, the impact of including air between the beam and the DUT as well as side effects due to the simulated geometry were explored. It was found that none of these sources can provide a substantial enough impact on the SEU cross-section to reconcile the anomalous measurement made at TAMU.

Contents

List of Figures

List of Tables

Chapter 1

Introduction

Many areas of the Large Hadron Collider (LHC) are equipped with commercial electronics that are not specifically designed to be radiation tolerant. An extensive and accurate understanding of how these electronics behave in the radiation field of high-energy hadron colliders is crucial for the continued acceptable operation of the LHC. The mixed-radiation field present and subsequent radiation induced errors in the electronics must be modelled, monitored, and mitigated in order to ensure the longevity and robustness of the experiment. This is the goal of the Radiation to Electronics (R2E) project at the LHC [1].

One mechanism through which this radiation field can damage electronics is through single event effects (SEEs). For the CMOS technology considered in this study, SEEs manifest most commonly as either single event latchups (SELs) or single event upsets (SEUs). The former is a hard error that occurs in a device and causes permanent damage whereas the latter is a soft, temporary error such as a bit flip in a memory cell.

The mixed-radiation field present at various areas of the LHC has been accurately measured [2] and reproduced in simulations [3]. The primary sources of radiation in this field that are relevant to the electronics at the LHC come from beam losses in collimators, particle debris from hadron and heavy ion collisions, and interactions of the beam with residual gas in the pipe [2]. The energy spectra for a typical LHC underground zone is shown in fig. 1.1. Although this radiation field is dominated by neutral and singly-charged hadrons, inelastic collisions of these particles with material in and around the electronics results in the production of a variety of fragments and recoils. These secondary particles can pass through or near the sensitive volumes of vulnerable electronics and cause SEUs. These High Energy Hadron (HEH, defined as hadrons above 20 MeV) induced SEUs are extremely important in accelerator environments and they are the focus of the study presented herein.

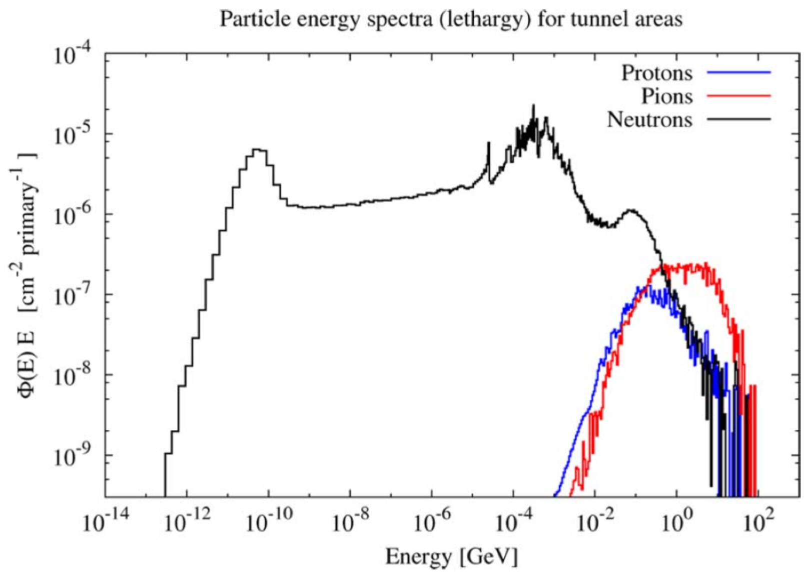

FIGURE 1.1: Particle energy spectra for a typical LHC tunnel area [2]. Specifically, this is the simulated radiation field produced by particle debris induced by proton-proton collisions at an interaction point and normalized to one collision.

Experimentally, heavy ion induced SEUs have been studied at a number of facilities. In this paper we consider the observations of many of these facilities that were made using the ESA SEU Monitor, a reference standard for SEU testing [4–7]. Our goal is to establish a physically consistent model for simulating SEUs that can explain the observed behaviour of heavy ions of various species and energies while maintaining validity for hadron induced effects.

Chapter 2

Background

2.1 Linear Energy Transfer

As high energy ions pass through materials they deposit energy through Coulombic interactions with atomic electrons and leave an ionization track [8]. In nuclear physics the energy loss of an ion as it traverses a medium is quantified in terms of the average energy loss per unit path length, i.e. the stopping power. A more commonly used metric in the world of Single Event Effects (SEEs) is the linear energy transfer or LET.

$$\text{LET} = -\frac{1}{\rho}\frac{dE}{dx} \tag{2.1}$$

where ρ is the density of the target material (typically in mg/cm^3) and dE/dx is the ion energy loss per unit path length (MeV/cm). The units of LET are then MeV/(mg/cm^2).

The LET of a given heavy ion is not constant as the ion travels through a material. The dE/dx of the ion is energy dependent, as shown in fig. 2.1, and as it traverses a medium it loses energy. This can clearly be seen in fig. 2.2 which shows a dependence of the specific ionization, which is proportional to the LET of the ion, as a function of the depth of penetration. At some depth in the material, the ion has lost enough energy that it is at the peak of its dE/dx in fig. 2.1 and thus is at a maximum in LET as shown in fig. 2.2. This spike is characteristic of all charged particles traveling through materials and is known as the "Bragg Peak". This behaviour is fundamental in heavy ion radiation therapy since it provides a mechanism for targeted energy deposition which allows for the radiation of a tumour while minimizing damage to surrounding tissue [9].

When it comes to understanding how heavy ions cause upsets in electronics it is important to consider that as the ions travel further through the material they will lose

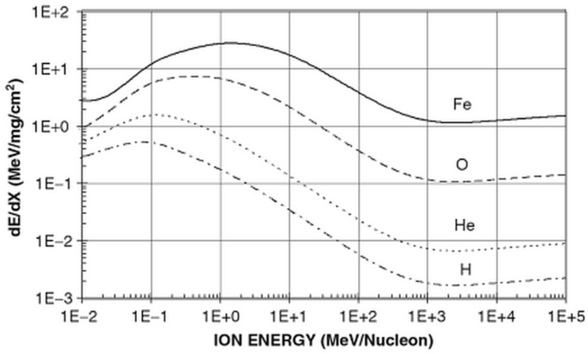

FIGURE 2.1: The energy loss rate per unit path length through silicon is shown for various heavy ions [8].

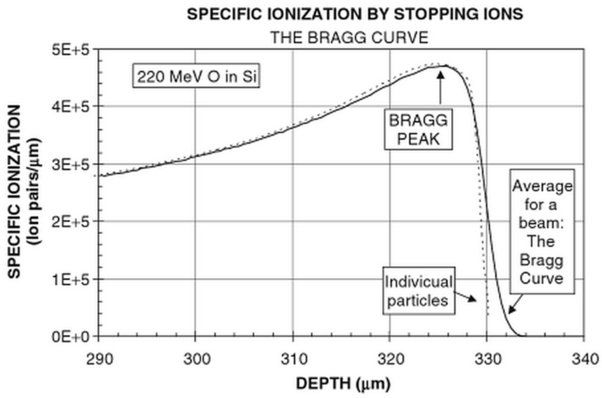

FIGURE 2.2: An increase in specific ionization, which is $\propto$ dE/dX, is clearly seen for 220 MeV O in Si as it travels deeper into the medium and loses energy [8].

energy and consequently have their LET increase as they travel (provided that they are initially to the left of the Bragg Peak). This could potentially cause an increase in the number of SEUs depending on the depth at which sensitive volumes are located in the electronics or whether there is material placed before them through which heavy ions can lose energy and increase their LET.

Typically LET is taken as the sole parameter to characterize the beam in SEU cross section experiments but there has been a great deal of research suggesting that ion species and energy may also need to be taken into account [8, 10, 11]. Different ions with different energies could have very similar LET values but result in quite different SEU cross sections. This is primarily the case at/below the LET threshold of a device suggesting that the ion species and energy is playing a role in indirectly induced SEUs caused by nuclear interactions. This change in the number of indirect SEUs would not be evident in the above threshold region (dominated by direct ionization events) but would play an important role when the number of direct ionization events decreases (sub-threshold).

2.1.1 Volume-Equivalent Linear Energy Transfer

The LET of an ion characterizes the energy *lost* per unit path length whereas we will refer to the volume-equivalent LET ($\mathrm{LET_{vol}}$) of an ion as the energy *deposited* per unit path length in a defined volume.

$$\mathrm{LET_{vol}} = -\frac{1}{\rho}\frac{\mathrm{E_{dep}}}{t} \tag{2.2}$$

where ρ is the density of the target material, E_{dep} is the energy deposited in the volume and t is the thickness of the volume.

LET and LET_{vol} are not necessarily the same. For example, the energy lost by an ion traveling through a device could manifest itself through energetic delta rays that escape the defined volume. The LET_{vol} will then be less than the LET of the ion. Also, LET_{vol} would take differences in the LET over the path through the SV into account. The difference between these two values is critical when evaluating SEUs in electronics. In particular, single event upsets in SRAM devices are caused by energy deposition in some defined sensitive volume (where the bit information is stored). This localized energy deposition will depend directly on the volume-equivalent LET of the incident ion as opposed to its LET.

2.2 Single Event Upsets

A charged particle traversing through any semiconducting material loses energy through Coulombic interactions. The particle slows down as it transfers its energy through the production of an ionization trail of free electron-hole pairs. These mobile charge carriers are then free to deposit energy in unwanted regions of the semiconducting materials [8]. If the charge is deposited in a region that stores information (i.e. the sensitive volume in an SRAM device) then a bit flip can occur wherein a $0 \rightarrow 1$ or a $1 \rightarrow 0$. This is what is known as a single event upset (SEU).

2.2.1 SEU Cross-Section

The idea of a cross section can be extended from nuclear physics to describe single event effects. The single event upset cross section, σ_{SEU} is typically defined as

$$\sigma_{SEU} = \frac{N_{SEU}}{\Phi \cdot N_{bit}} \tag{2.3}$$

where N_{SEU} is the number of single event upsets that occur, Φ is the total incident particle fluence, and N_{bit} is the number of bits.

A bit will flip when a certain, critical amount of charge is deposited in the sensitive volume (memory cell) of a device. Since the deposited charge is related to the amount of energy deposited in a volume and the thickness of the sensitive volume is constant, then there is a direct relationship between charge deposited and LET_{vol}. If there is a critical amount of charge that needs to be deposited in order for an upset to occur we would expect that there is a minimum LET_{vol} that must be surpassed in order to achieve a non-zero σ_{SEU}. It turns out this is only partially true as can be seen in fig. 2.3. Instead we see a gradual turn on of the cross section curve with increasing LET. This was found to be due to intra-cell variations in charge collection efficiencies [12]. Additionally, below this threshold SEUs are still occurring, albeit at rates much lower than above the turn on. This behaviour is discussed below.

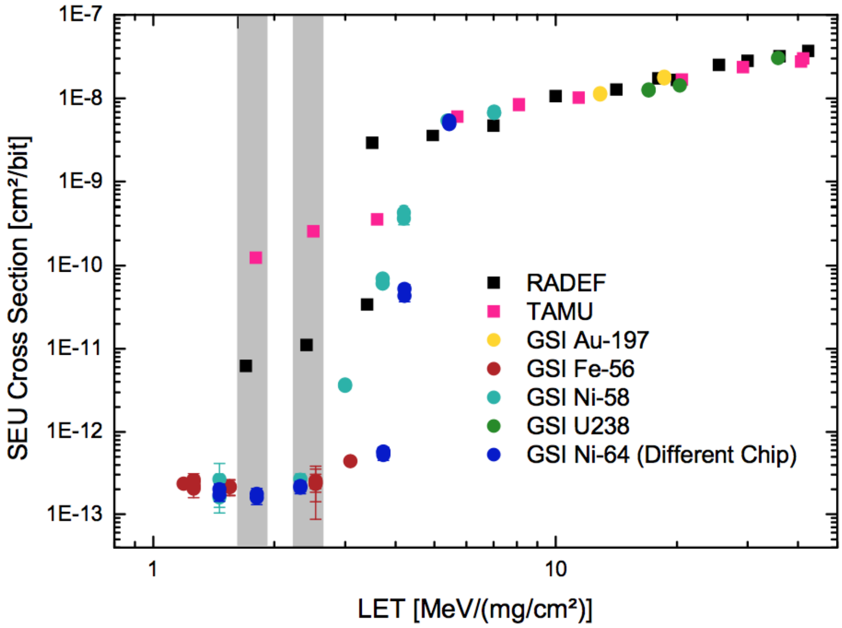

FIGURE 2.3: Experimental data from RADEF, TAMU, and GSI showing the measured SEU cross-section as a function of LET. Error bars are smaller than the symbol sizes [13].

2.2.2 Coulombic Interactions

Figure 2.3 shows experimental observations of SEU cross-sections for the ESA SEU Monitor. Experiments were performed at three different facilities (GSI, RADEF, and TAMU) with several different ions in order to see how σ_{SEU} varies with LET. The GSI ions had energies between 50 MeV/u and 1500 MeV/u whereas the TAMU ions were at 25 MeV/u and the RADEF at 10 MeV/u. We quantify the turn on region with a threshold LET value, above which the SEU cross-section appears to saturate. In this case the LET threshold appears to be somewhere between 3 and 4 MeV/(mg/cm^2).

Above the LET threshold the cross sections at all facilities are in agreement. This is where Coulombic interactions between the ions and the semi-conductor lattice are strong enough to trigger SEUs. These upsets are thus caused by direct ionization of the sensitive volume by the incoming heavy ions. These interactions are independent of the ion energy and species, to first order, and the cross section can be entirely quantified in terms of LET.

2.2.3 Nuclear Interactions

We would expect that below the LET threshold (corresponding to the deposition of a critical amount of charge Q_{crit} in the sensitive volume) ions would no longer be able to cause any single event upsets. However, we see that ions with LET below the threshold also appear to be causing upsets. In addition, there is a very obvious energy dependence of σ_{SEU} in this region which can be clearly seen at LETs of 1.8 and 2.4 MeV/(mg/cm^2). It appears that there is an initial increase of σ_{SEU} with ion energy and then a decrease as we approach the even higher energies at GSI. This is shown in fig. 2.4. A σ_{SEU} increase of over a factor of 10 between 10 MeV/amu and 25 MeV/amu at an LET of 5 MeV/(mg/cm^2) was also previously reported for a 0.5 μm bulk SRAM [10].

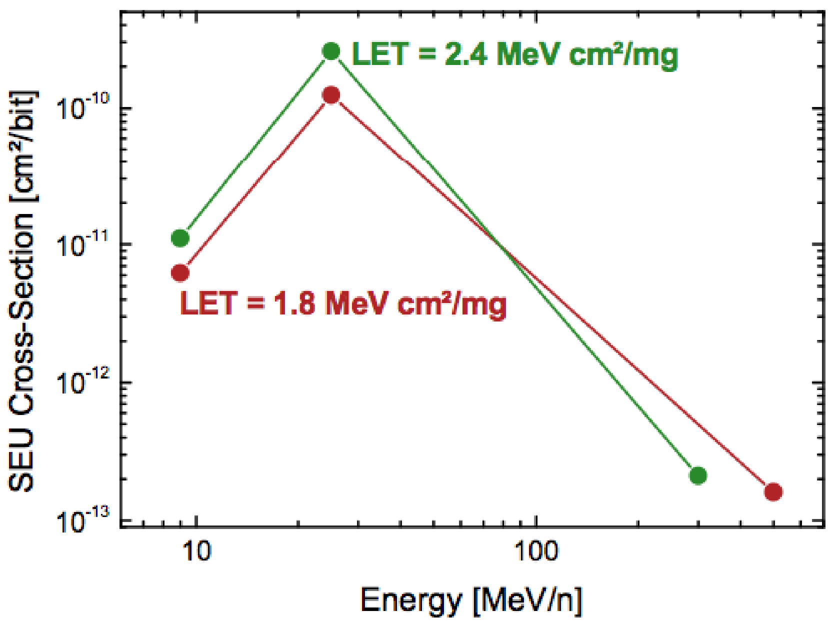

FIGURE 2.4: Observed energy dependence of the SEU cross-section as a function of ion energy in the sub-threshold region [13].

This region is where nuclear reactions have become dominant. The incoming ions no longer have sufficient LET to cause SEUs through direct ionization. However, incoming ions can still have nuclear interactions with the atoms in the semiconductor lattice and produce new ions, with larger LETs, that are capable of ionizing the medium and causing an upset. The probability of an inelastic nuclear interaction occurring for a given ion in a certain material is quantified through the corresponding inelastic cross section or inelastic interaction length. For example, the inelastic interaction length of a 25 MeV/amu 22Ne ion in silicon is 9.3 μm, meaning that the probability that an interaction occurs in 1 μm (typical SEU sensitive size) is $\sim 10^{-5}$. These nuclear reactions do have a dependence on incident ion energy and so we begin to see behaviour that was overwhelmed by the number of direct ionization induced upsets in higher LET region.

Chapter 3

Experimental Data

3.1 ESA Monitor

The experimental data explored in this study was collected with the ESA SEU Monitor. The monitor uses 250 nm technology, 4 Mbit SRAM and was produced as reference standard for SEU testing [4–7]. In order to count the number of SEUs that occur in the monitor, a known bit pattern is first written to the device before it is irradiated. After irradiation, the bit pattern can then be read out and the number of bit flips that have occurred provides the measurement of the number of single event upsets.

3.2 Facilities

In this study we look at experimental observations from 4 different facilities. Our highest energy dataset comes from the GSI Helmholtz centre for heavy ion research in Germany [14]. These ions have energies ranging from 50 to 1500 MeV per nucleon. Additionally we take into account data coming from the cyclotron at UCL [15] and the RADEF facility in Finland [16]. These two facilities produce heavy ions with energies on the order of 10 MeV per nucleon. Finally, our intermediate dataset comes from the cyclotron at TAMU in Texas [17] which produces ions at energies of 15 MeV/u and 25 MeV/u [18].

3.3 Experimental Heavy Ion Induced SEU Observations

The full set of experimental data considered in this study is shown in fig. 3.1.

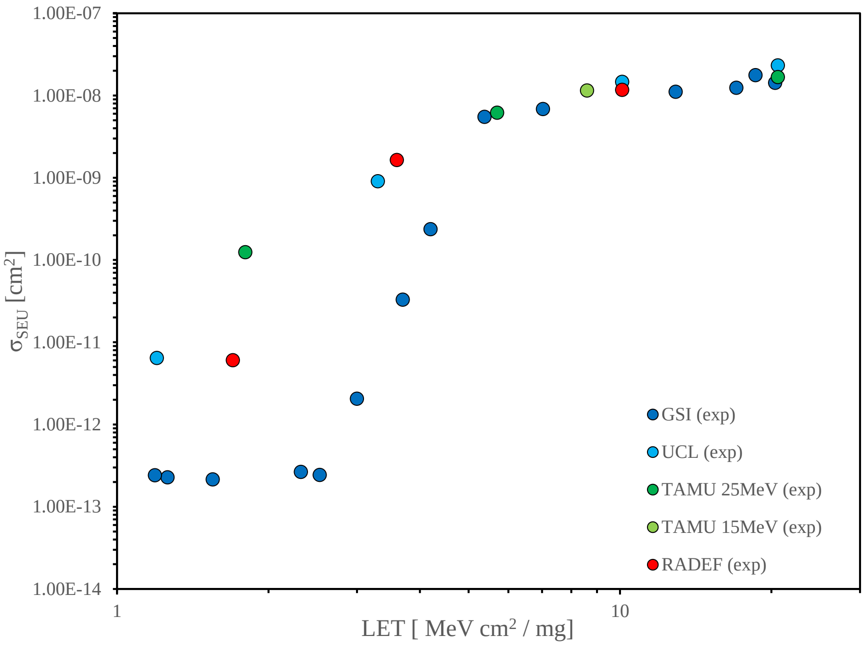

FIGURE 3.1: Full set of experimental σ_{SEU} data considered in this study. The data comes from GSI, RADEF, TAMU, and UCL. The GSI results for very similar ions and energies are merged. Error bars are smaller than the symbol sizes, however all results were obtained with measurements of more than 100 SEUs corresponding to a maximum statistical error of 10%.

In the region above the LET threshold we see strong agreement between the measurements of the various facilities. In the knee region (LET of $\sim 2.6 - 4.5$ MeV cm^2/mg) we see large discrepancies begin to pop up between measurements at difference facilities. This is seen more clearly in fig. 2.3 where more data of the knee region is included. In fact, in this region, experimental measurements of σ_{SEU} for the same ion at the same facility have cross sections that differ by an order of magnitude or more. This is attributed to the sensitivity spread amongst the devices.

In the region below the LET threshold we see a plateau region at low LET values where σ_{SEU} is dominated by nuclear interactions. In this region σ_{SEU} no longer correlates with LET. It appears that the SEU cross-section for an ion of roughly the same LET at about 1.6 MeV/(mg/cm^2) varies by more than 3 orders of magnitude depending on the ion energy. This behaviour is explored in this study.

3.4 Benchmark Proton Data

In additional to the experimental heavy ion data we consider two sets of experimental measurements of the σ_{SEU} for incident protons of different energies. One set comes from [4] and the other from a combination of measurements taken by an R2E team at PSI in Switzerland and at TRIUMF in Canada. The reason that there are two sets of measurements is that the ESA SEU monitor used by CERN was found to have a 230 MeV proton SEU cross-section (2.6×10^{-14} cm^2/bit) that was 25% lower than that initially calibrated by ESA in 2004 (3.4×10^{-14} cm^2/bit). This difference could be initially attributed to the part-to-part variation, however the spread amongst devices was shown to be very small. Through an internal communication with ATMEL (manufacturer of the ESA Monitor SRAM) it was suggested that an increase in the core voltage of the memory (from 2.5 to 2.7 V) could be the cause of the proton cross-section decrease. It is known that the heavy ion data from UCL, RADEF, and TAMU use the old ESA Monitor but it is unclear which monitor was used at GSI. Therefore we consider both data sets in our analysis.

A successful model for the simulation of heavy ion induced SEUs must also be consistent with hadron induced effects and so we use the proton data as a benchmark throughout this study.

Chapter 4

Simulating Energy Deposition

4.1 FLUKA

FLUKA is a Monte Carlo particle transport simulation package. It has applications ranging from radiation shielding to medical physics to telescope design [19]. We use FLUKA to simulate the transport of particles incident on the ESA SEU monitor through its SRAM memory sensitive volume (SV) and surrounding material. The output of FLUKA is the energy deposition spectrum of the incident particles being simulated. In particular we obtain a spectrum of the energy deposited in a single sensitive volume of the SRAM memory. Our goal is to recreate the experimental results obtained at GSI, UCL, RADEF, and TAMU by simulating not only heavy ion direct ionization of the material but also nuclear reactions (which play a large role in the sub threshold region).

4.2 Geometry

In order to use FLUKA to simulate the transport of particles through the ESA SEU monitor the geometry of the monitor itself must first be implemented. It is impossible to simulate the entire 4Mbit geometry of the monitor in detail due to computational limitations so this study is performed using only a small section of the detector that contains only a few memory cells (sensitive volumes).

The sensitive volumes of the ESA SEU monitor (i.e. drains of the OFF transistors in the memory cells) have physical dimensions of roughly 0.4 μm x 0.4μm x 0.2μm. However, heavy ions do not have to pass directly through this physical volume in order to cause an SEU. Contributions to SEUs come not only from energy deposition in the sensitive volume itself but also from diffusion of electron hole pairs that are created outside of the sensitive volume and drift to deposit their charge inside. These effects contribute to an effective sensitive volume that is larger than the physical volume.

4.2.1 Nested Volume

In order to account for this extended sensitive volume a nested volume geometry could be implemented [20]. This is characterized by several nested regions each with different charge collection efficiencies. The nested regions can then be defined such that the charge collection efficiency falls off with distance from the physical sensitive volume. For example, heavy ions directly passing through and ionizing the innermost sensitive volume could have 100% charge collection efficiency whereas those passing through a region immediately outside this volume could have 50% charge collection efficiency and so on. The sizes of the regions and the charge collection efficiencies themselves are determined empirically by fitting to known, consistent experimental data (i.e. cross section data above the LET threshold). The problem with this approach is that in order to get an accurate estimate for σ_{SEU} of various heavy ions, a large number of nested regions must be implemented. This makes the approach very computationally intensive and not very versatile. Additionally, the calibration to the heavy ion data is not straight-forward. For these reasons we explore an alternative model in this study.

4.2.2 IRPP

We have implemented a less computationally intense model, known as the integrated rectangular parallelepiped (IRPP) model, wherein we have a single region that we irradiate with flux from different heavy ions. The geometry for this model is shown in figs. 4.1 and 4.2. This single region has been repeated 16 times in our geometry to make up a 16 bit fragment of the 4 Mbit SRAM memory of the ESA SEU monitor. The lateral surface of the SV is equal to the heavy ion saturation cross-section of $10\mu\text{m}^2$, which is also the cell size as multi-bit upsets (MBUs) hardly play a role in the total SEU cross-section.

For a specific ion, our simulation records the event by event energy deposition in the sensitive volumes. The result that we get from the simulation is the probability that an event deposits a given amount of energy in the sensitive volumes. The simulation does not tell us whether or not an upset was caused. We then convert the energies to LET values and then look at the experimental data to see what the experimental SEU cross section for the device is at that LET. These cross sections can then feed back into the analysis to weight the energy deposition events, effectively accounting for the probabilities that given energy depositions would cause an upset in the device. This is again a semi-empirical model wherein we are only getting information about energy

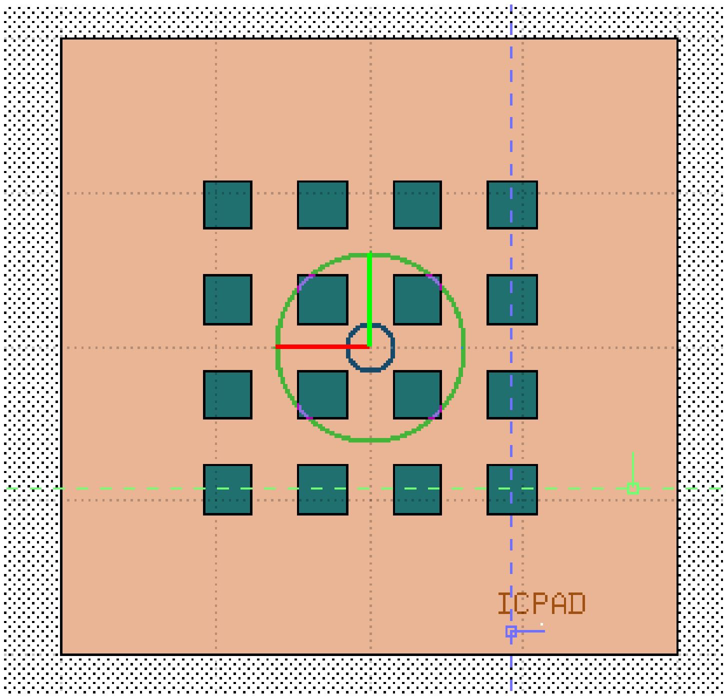

FIGURE 4.1: Cross sectional view of the geometry implemented in FLUKA showing the 16 sensitive volumes.

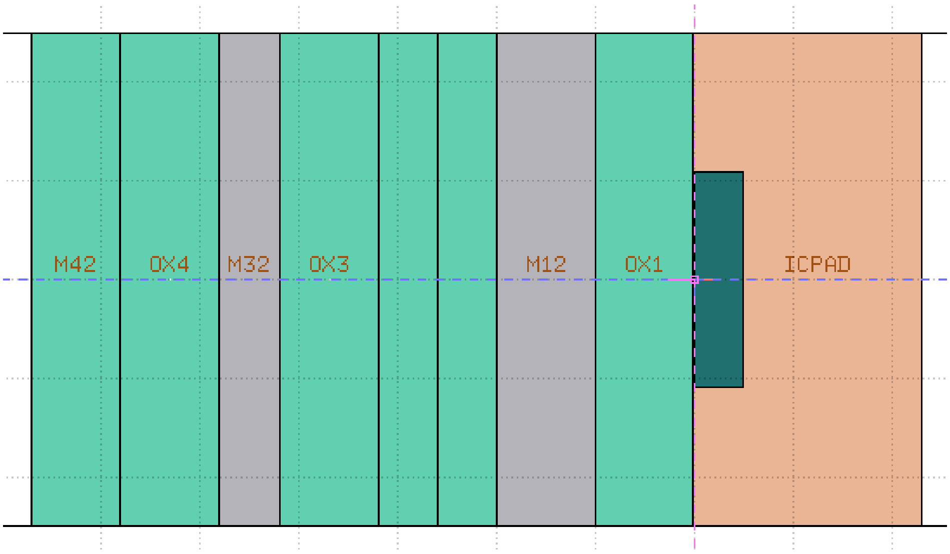

FIGURE 4.2: Side view of the geometry implemented in FLUKA showing the back end of line (BEOL) and a single sensitive volume.

deposition from the FLUKA simulation but how the energy deposition translates into probabilities for having a SEU comes from the experimental data.

4.2.3 Sensitive Volume Thickness

As mentioned previously, the effective size of the sensitive volume is larger than its physical size. This is because diffusion effects extend the range through which ionization of the medium can cause charge collection in the physical sensitive volume. In our IRPP model we do not have nested volumes that can account for the diffusion effect. Instead, we will perform simulations of incident protons on the ESA SEU monitor and vary the thickness of the sensitive volume, similarly to what was initially performed in [21], such that our simulation best matches the benchmark proton data. This would be the sensitive volume thickness of the ESA SEU monitor that we could then use in our heavy ion simulations.

4.2.4 Back End of Line

The back end of line (BEOL) consists of a layer of material before the sensitive volume in the ESA SEU monitor. Heavy ions must pass through this layer before entering the device and can be slowed down by interaction with this extra material. This could result in a shift of the ion LET towards the Bragg Peak, increasing the probability of inducing an SEU. Furthermore, the possibility for nuclear interactions with this additional material will increase the SEU cross-section in the sub-threshold region. We know from the manufacturer that this BEOL consists of a 6.7 μm thick layer of SiO_2 (insulator) and aluminum (metal). Still, for completeness we simulate the impact of larger BEOLs. It could be that with a thick enough BEOL, enough additional nuclear interactions are induced that σ_{SEU} increases by several factors. Understanding the dependence of σ_{SEU} on BEOL thickness is a goal of this study.

4.2.5 Substrate

In addition to the BEOL that is placed before the sensitive volume, there is also a substrate on which the sensitive volumes are mounted in the production of the SRAM. This substrate is located directly behind the sensitive volume. The thickness of this substrate is typically several hundred μm, however in order to reduce our CPU time we only simulate 2.3μm of this substrate. Clearly, since the substrate is located behind the sensitive volume it cannot have an impact on direct ionization induced SEUs. However, incident ions still have the ability to participate in nuclear interactions with this material and if a secondary ion backscatters it can cause additional SEUs in the device. It is important to understand this behaviour for low LET ions where, depending on the angular distribution of secondaries, this backscattering could potentially have an impact on the SEU cross section and our simulation of only 2.3μm could underestimate the cross-section.

4.2.6 Air

Of the experimental data considered herein, only the experiments performed by UCL and RADEF were done in a vacuum. At GSI the heavy ions traveled through 1 meter of air before hitting the ESA Monitor and they traveled through 2 cm of air at TAMU. In addition to the tests done in vacuum by RADEF that we consider in this study, tests were also performed for the same ion with 1 cm and 3 cm of air before the DUT [18]. This additional air in front of the device could impact the SEU cross section in the same manner as the back end of line as it is simply an additional material that the heavy ions must travel through before entering the device. In order to perform an accurate analysis of low LET SEU cross sections, this air must be taken into account.

4.2.7 Side Effects

Since we are only simulating a small section of the ESA SEU monitor we are imposing a systematic bias in our results for the sub-threshold region wherein the simulated SEU cross sections could be systematically lower than they are in reality. The reason for this is that a nuclear reaction could occur in some region of the simulated geometry and send a high LET particle flying through the device at a non-zero angle to the initial beam. If this angle is large enough then the secondary particle will miss the sensitive volume initially in the path of the primary ion. In reality, this secondary would go on to cause an upset in a sensitive volume along the new path but in our simulations we may not have that particular sensitive volume implemented in the geometry. For example, if we only have 1 sensitive volume simulated and we direct our incident primary ions towards this region, secondary ions created will fly off at some angle to our primary beam and miss the sensitive volume entirely. It will appear to us that these do not cause upsets when in fact they would if we had simulated a larger geometry. It is impossible to simulate all 4 Mbit of sensitive volumes in the ESA monitor but we will simulate the impact that the size of the geometry has on ions of various energies at low LET. In particular we will look at the impact of reducing our geometry to only include 1 sensitive volume (fig. 4.3) and extending it to include 400 sensitive volumes (fig. 4.4). We expect that the impact of these side effects on σ_{SEU} should saturate as we approach a larger number of sensitive volumes.

4.3 Delta Rays

When an energetic charged particle passes through the semiconductor lattice some electrons can be knocked out of their orbit at high velocities. These electrons are known as

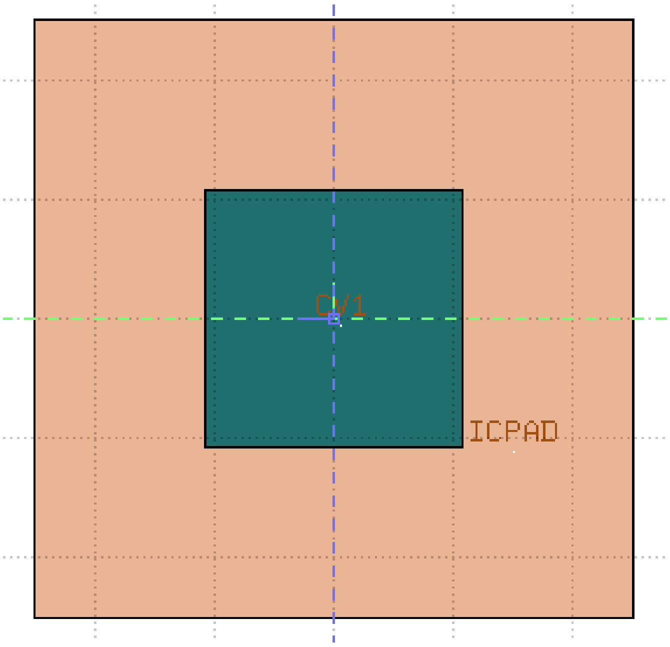

FIGURE 4.3: Cross sectional view of the geometry implemented in FLUKA with only 1 sensitive volume.

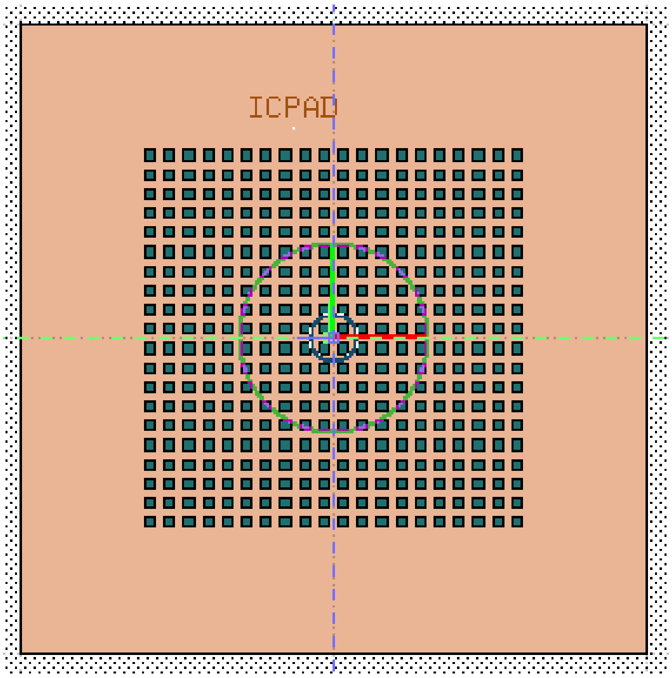

FIGURE 4.4: Cross sectional view of the geometry implemented in FLUKA with 400 sensitive volumes.

delta-rays and play a crucial role when it comes to energy deposition in semiconductor devices. They can not only deposit their own energy in and around the sensitive volume but, with high enough energies, they can cause secondary ionizations on their own. This can sometimes cause a shower of further delta rays (especially when in the presence of an accelerating electric field).

When simulating delta ray production and energy deposition in FLUKA, thresholds are put in place to prevent the production of delta rays below some energy threshold as well as stop the transport of delta rays when their energy drops below a certain threshold. These thresholds are necessary in order to limit the CPU time that the simulations will take. Delta rays that are in the sensitive volume will need to have a lower production/transport threshold since their local energy deposition can cause a dramatic increase in the SEU cross section if not simulated correctly. For example, if the transport threshold was set too high, delta-rays produced in the sensitive volume would be simulated to immediately deposit all of their energy in the volume, thus causing a higher number of upsets than would be seen in reality. There is a compromise between accuracy and CPU time that must be met. However, delta-rays produced outside of the sensitive volume could have higher thresholds set since their energy deposition is not as relevant when it comes to σ_{SEU}.

Physically, the maximum energy that delta rays could have is directly related to the energy of the primary particle per nucleon that knocked the electron out of its orbital.

The most energetic delta ray produced by a primary particle will have an energy approximately equal to the energy per nucleon of the primary divided by 500 [22]. Because of this, delta-rays play a much more important role when looking at the high energy per nucleon heavy ions produced at GSI, especially at low LET. The high energy delta rays produced by these heavy ions can play an even more significant role than the direct ionization of the heavy ion itself (since it is low LET) and a realistic simulation of the production and transport of these delta rays is necessary in order to recover a realistic SEU cross section.

4.4 Computation Time

A severe limitation of these simulations is the sheer computational intensity of propagating millions of incident heavy ions, as well as the delta rays and secondary ions that they produce, through the geometry of the ESA Monitor implemented in FLUKA. Although we only perform the simulations for a small section of the ESA monitor with only a few sensitive volumes, the simulations for each case of each heavy ion could take several days. There are two primary mechanisms through which we attempt to reduce the computation time of these simulations: by setting delta ray production and transport thresholds and by introducing biasing of nuclear interactions.

4.4.1 Delta Ray Thresholds

We set the delta ray production threshold outside of the sensitive volumes to 10 MeV. This means that, outside of the sensitive volumes, only delta rays that would be produced with more than 10 MeV of energy are actually generated by FLUKA. Again, this is fair because delta-rays typically do not have enough energy to induce a SEU and the contribution of electrons generated outside the sensitive volume can be considered as negligible. The production threshold inside the sensitive volumes is set to 1 keV.

In order to see the impact of the delta-ray transport threshold on our simulated cross sections we ran simulations using global transport thresholds of 10 MeV and 1 keV. The results for 56Fe at 996 MeV (LET = 1.26 MeV/(mg/cm^2)) are shown in fig. 4.5.

We can clearly see that with a threshold of 10 MeV there are many more events with large energy deposition which would cause an artificial inflation of the SEU cross section. This occurs because the delta-rays that are produced in the sensitive volumes have energies below the transport threshold and thus are simulated to have all of their energy deposited locally. In reality these delta rays would move out of the sensitive volumes before depositing all of their energy.

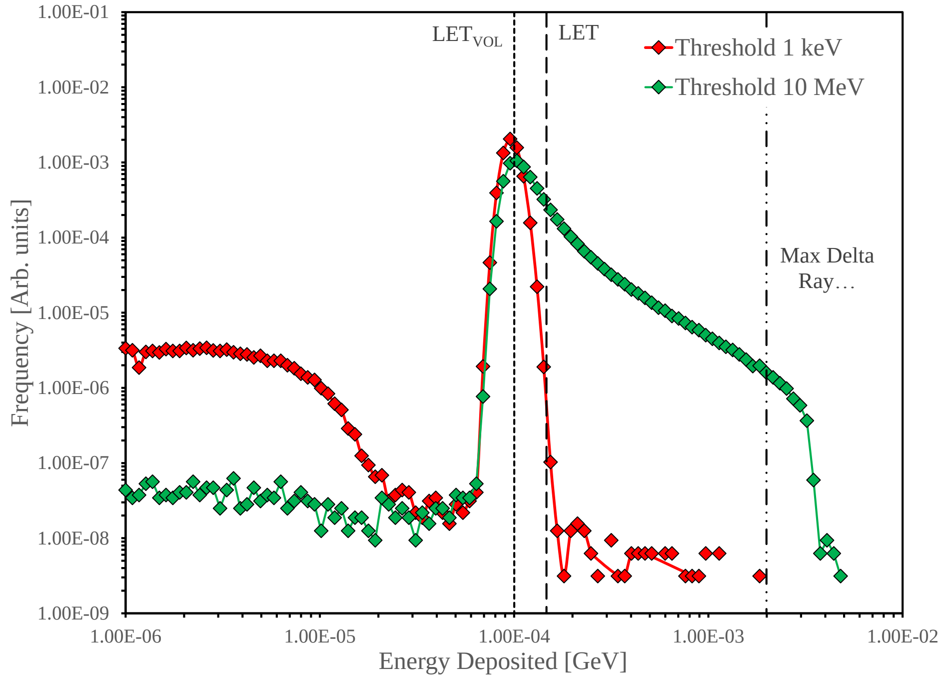

FIGURE 4.5: Energy deposition spectrum for 56Fe at 996 MeV/u (LET = 1.26 MeV/(mg/cm^2)) for both a delta-ray threshold of 10 MeV and 1 keV. The LET, effective LET, and maximum delta ray energy for the ion are marked.

When the threshold is reduced to 1 keV we see that the tail of the spectrum towards higher energy deposition (caused by local energy deposition of delta rays) disappears and we have a much narrower distribution at high energies. This narrow peak is the energy deposition caused by direct ionization of the medium. Additionally, a cluster of high frequency events with much lower energy deposition appear below 20 keV. These correspond to delta-rays that are transported through the sensitive volume and only deposit a small fraction of their energy there as they pass through. The infrequent events with deposited energy greater than 200 keV are caused by nuclear interactions.

Clearly, the delta-ray transport threshold inside the sensitive volume needs to be set very low in order to accurately simulate the energy deposition spectrum of the incident ion. However, the transport threshold outside of the sensitive volume does not appear to be very important since the energy deposition of delta rays that are transported through the sensitive volumes is very low and will not contribute to our SEU cross-section. We performed simulations varying the transport threshold outside of the sensitive volume and measured the computation time for these simulations to see if we could speed up our computations without losing accuracy. The results are tabulated in table 4.1.

Transport Threshold (Outside SV)	σ_{SEU} [$\times 10^{-14}$ cm^2]	Computation Time [Hours]
1 keV	9.5 ± 0.7	17.8
1 MeV	8.3 ± 0.7	16.1
10 MeV	8.4 ± 0.7	16.1

Table 4.1: Computation times and SEU cross-sections for 56Fe at 996 MeV/u with varying delta ray transport thresholds outside of the sensitive volume.

Although the cross-sections that we get are not statistical discrepant for the different transport thresholds, the gain in computation time is insignificant with increasing transport thresholds outside of the sensitive volume. For this reason we perform our simulations with a delta-ray transport threshold set to 1 keV globally. In addition the production threshold is set to 1 keV within the sensitive volumes and 10 MeV outside of the sensitive volumes as discussed earlier.

4.4.2 Biasing

When simulating the SEU cross-section in the sub-threshold region, the dominating contribution comes from nuclear interactions. These nuclear interactions occur with a probability of roughly $10^{-5}/\mu$m. In order to get enough statistics to properly model SEUs in this sub-threshold region we would need to simulate a much larger number of primary particles than we would in the above-threshold case. In order to compensate for this we could implement inelastic collision biasing in FLUKA wherein the rate of inelastic interactions is increased by some factor for the purposes of simulation and then the energy-deposition is scaled down afterwards to account for the biasing.

The implementation of this has been extensively tested for protons and so we comfortably use biasing in our proton simulations. Biasing for heavy ion nuclear interactions has not yet been tested and so a short analysis was performed as part of this study. The resulting cross sections and computation times for different biasing factors are given in table 4.2. The biased and unbiased energy deposition spectra are shown in figs. 4.6 and 4.7.

Ion	Biasing Factor	σ_{SEU} [$\times 10^{-14}$ cm^2]	Computation Time [Hours]
56Fe @ 996 MeV/u	1	9.5 ± 0.7	17.8
56Fe @ 996 MeV/u	100	7.9 ± 0.7	0.30
13C @ 10.1 MeV/u	1	7.2 ± 0.2	22.8
13C @ 10.1 MeV/u	100	7.8 ± 0.2	0.25

Table 4.2: Computation times and SEU cross-sections for 56Fe at 996 MeV/u and 13C at 10.1 MeV/u with varying biasing factors for nuclear interactions.

Despite the computation time of the simulations decreasing significantly with biasing in place, the cross sections may potentially be discrepant within statistical uncertainties.

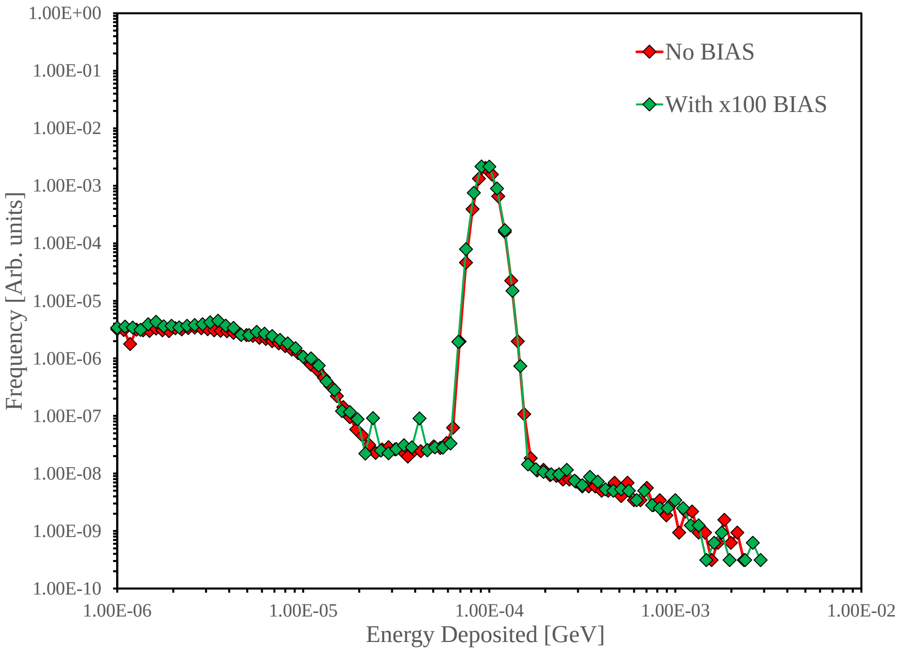

FIGURE 4.6: Biased and Unbiased Energy Deposition Spectra for 56Fe @ 996 MeV/u.

The results are currently inconclusive and more study needs to be done before the heavy ion biasing can safely be used. For this reason we avoid its implementation in our study.

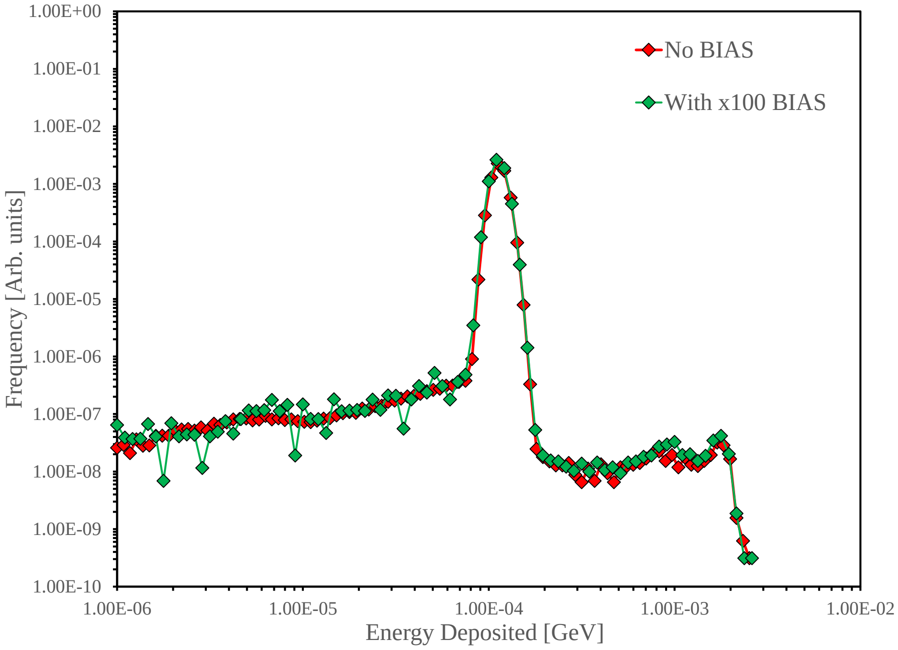

FIGURE 4.7: Biased and Unbiased Energy Deposition Spectra for 13C @ 10.1 MeV/u.

Chapter 5

Recovering SEU Cross-Sections

5.1 IRPP Model

The FLUKA simulations of each heavy ion beam tell us how much energy is deposited in the sensitive volumes by each event, with one event referring to the generation of one incident particle. Given an LET threshold for SEUs (coming from experimental data) we can convert to an energy threshold using (2.1). Only the ions that deposit an energy greater than the threshold have the possibility to induce an SEU.

The simulated SEU cross-section per bit in the device is defined as

$$\sigma_{SEU} = \frac{N_{SEU}}{\Phi} \tag{5.1}$$

where N_{SEU} is the number of single event upsets that occur and Φ is the total incident particle fluence. This can be written as

$$\sigma_{SEU} = \frac{n \int_{E_{crit}}^{\infty} w(E) \cdot \epsilon(E) \, \mathrm{d}E}{\frac{n}{S_{beam}}} = S_{beam} \int_{E_{crit}}^{\infty} w(E) \cdot \epsilon(E) \, \mathrm{d}E \tag{5.2}$$

Where n is the number of incident particles, E_{crit} is the critical amount of energy that needs to be deposited for a non-zero SEU probability which comes from converting the LET threshold using (2.1), $\epsilon(E)$ is the energy deposition density function (i.e. the probability that a generated particle in the simulation will deposit an energy E in the sensitive volume), $w(E)$ is a response function built from the experimental heavy ion data, and S_{beam} is the surface area of the incident ion beam. Effectively, $w(E)$ gives the probability that an event that deposits a some amount of energy will cause an SEU in the device. We then have a semi-empirical model where FLUKA gives us the energy deposition spectrum $\epsilon(E)$ and we build our response function $w(E)$ from the experimental data (discussed below) which tells us what the probability is of an event that deposits a given energy to cause an upset.

5.2 Calibrating a Response Function

We build our response function out of a 4-parameter Weibull function of the form

$$w(E) = \sigma_{SAT}\left(1 - e^{-\left(\frac{E-E_0}{w}\right)^s}\right) \tag{5.3}$$

where σ_{SAT} is the saturation value of the SEU cross section, E_0 is the threshold energy that needs to be deposited for an SEU to occur, w is the width parameter and s is the shape parameter [23].

In order to reproduce the experimental data from GSI, UCL, TAMU, and RADEF in the region above the LET threshold, we do a least squares fit of our simulated cross-sections to the experimental cross-sections using the 4 free parameters of our Weibull function $w(E)$. The resulting Weibull parameters are given in table 5.1 and the cross-section results are shown in fig. 6.3. The simulated points above the threshold fit the data very well but there is a clear discrepancy in the knee region. This extreme sensitivity at the knee is due to variations in the critical charge across different components of the detector which smears the threshold LET region as there is no longer one specific critical charge that must be deposited for an SEU to occur.

Parameter	Value
σ_{SAT}	3.72×10^{-8} cm^2
E_0	0.35 MeV
w	21.78 MeV
s	0.66

Table 5.1: Weibull parameters obtained by a least squares fit of the simulated cross-sections to experimental cross-sections in the above threshold region.

Note that although there is strong agreement between the simulation and the data there is a mismatch between the response function and the data. This is due to the fact that the experimental SEU cross-sections were quoted in terms of their LET but our simulations give us a volume-equivalent LET. As discussed in chapter 2, this volume-equivalent LET is lower than the LET of the ion at the surface of the DUT for direct ionization of normally incident particles. Thus, if we were to weight the simulated energy deposition spectra of the heavy ions using a response function that was fit to the

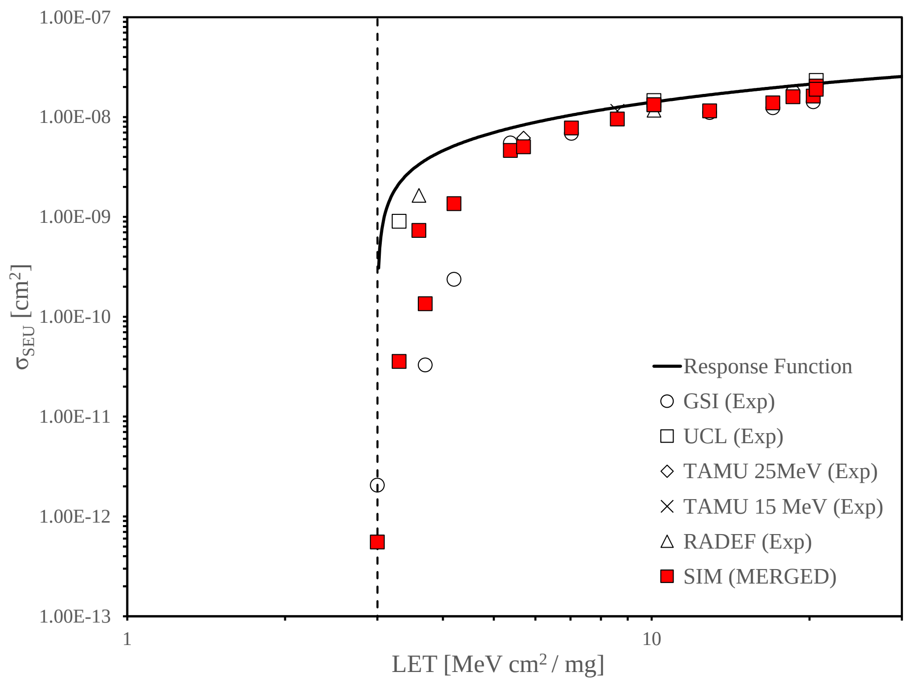

FIGURE 5.1: Experimental cross-section values for the ions above the LET threshold and the associated simulation values we obtained by empirically adjusting our response function. As expected, the values match very strongly in the above threshold region.

experimental data we would underestimate σ_{SEU}. Instead, the response function must be modified in order to account for the difference between the LET and deposited energy (or volume-equivalent LET). This is what is recovered by doing a least squares fit of our simulated cross-sections to the experimental cross-sections using the parameters of our Weibull function as fit parameters.

Additionally, in the knee region, small statistical variations in the energy deposition spectrum can cause drastic differences in the simulated σ_{SEU} because the response function is extremely sensitive in this area (due to its large derivative). Additionally, as discussed in 3, even experimental measurements made in this region of the same ion at the same facility can vary by an order of magnitude. For this reason the experimental and simulated points in this region used merged data for ions of very similar LETs.

5.3 SEU Cross-Section from Energy Deposition

Now that we have our response function calibrated we can easily translate from the energy deposition spectrum given to us by FLUKA to an SEU cross-section using the formalism of eq. (5.2). Although this was calibrated to the above threshold region, it can also be applied to heavy ions with LETs below the threshold as well as protons, which owing to the different energy deposition mechanism, are not used in the calibration. This is because protons and low LET heavy ions will deposit energy by engaging in nuclear interactions with the material in the device. This will result in secondary heavy ions with higher LETs than the incident particle which are capable of causing SEUs. FLUKA will then output an energy deposition spectrum which will contain a cluster of infrequently produced, high energy deposition events which will be weighted by the response function to account for their higher probability of inducing an SEU.

Chapter 6

Results

6.1 Proton Benchmarking

Our model should be able to consistently reproduce not only experimental heavy ion data but also proton induced SEUs. For this reason we benchmark our simulation against experimental proton data.

6.1.1 Determining the Effective Sensitive Volume Thickness

A plot of σ_{SEU} as a function of sensitive volume thickness for 230 MeV protons is shown in fig. 6.1. The experimental upper bound for σ_{SEU} pertains to measurements made of 230 MeV protons using the old monitor whereas the lower bound corresponds to measurements made with the new monitor.

From the figure we can see that σ_{SEU} for 230 MeV protons does not have a strong dependence on the thickness of the sensitive volume. As the thickness of the sensitive volume is increased, two competing effects come into play. First, with a larger sensitive volume, heavy ions and delta rays are now able to deposit more energy since they have a longer distance over which they can interact with the semiconducting material. This serves to increase the SEU cross-section. However, we see from eq. (2.1) that with a larger thickness our experimental values which are in terms of LET are translated to higher energy values. This effectively shifts our response function $w(E)$ to the right reducing the probability that a given amount of energy deposition will result in a SEU. This effect contributes to a reduction in the SEU cross-section. At larger thicknesses the gain from the former effect will be less pronounced and we see a consistent reduction in the cross-section as a function of sensitive volume thickness.

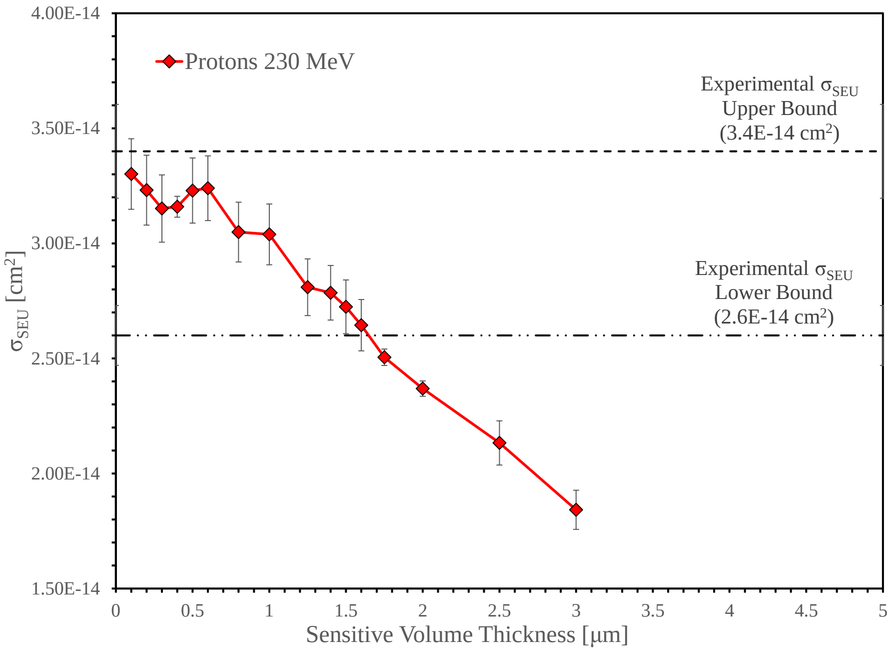

FIGURE 6.1: Simulated SEU cross-sections for 230 MeV protons as a function of sensitive volume thickness. The range of experimental cross sections for 230 MeV protons are shown as black, dashed lines.

Considering the fact that a sensitive volume thickness of 0.3 μm to 0.5 μm is more physical, the data suggests that the majority of the experimental data, to which our response function was fit, comes from the old monitor. However, even extending the sensitive volume thickness to 1.5 μm only results in less than a 30% decrease in σ_{SEU}. We take 0.5 μm as our thickness for the low-LET heavy ion simulations. This is a measure of the "effective thickness" of the sensitive volume taking into account both direct energy deposition in the physical sensitive volume and diffusion effects from the outside.

6.1.2 Energy Dependence

We saw in fig. 6.1 that a sensitive volume thickness of ~ 0.3 μm reproduces the experimental data taken with the old ESA monitor and a thickness of ~ 1.5 μm reproduces the data with the new monitor. If our model is physically consistent for both heavy ions and hadrons then we should be able to reproduce the experimental dependence of σ_{SEU} on proton energy. The results of our simulation are compared to experiment in fig. 6.2.

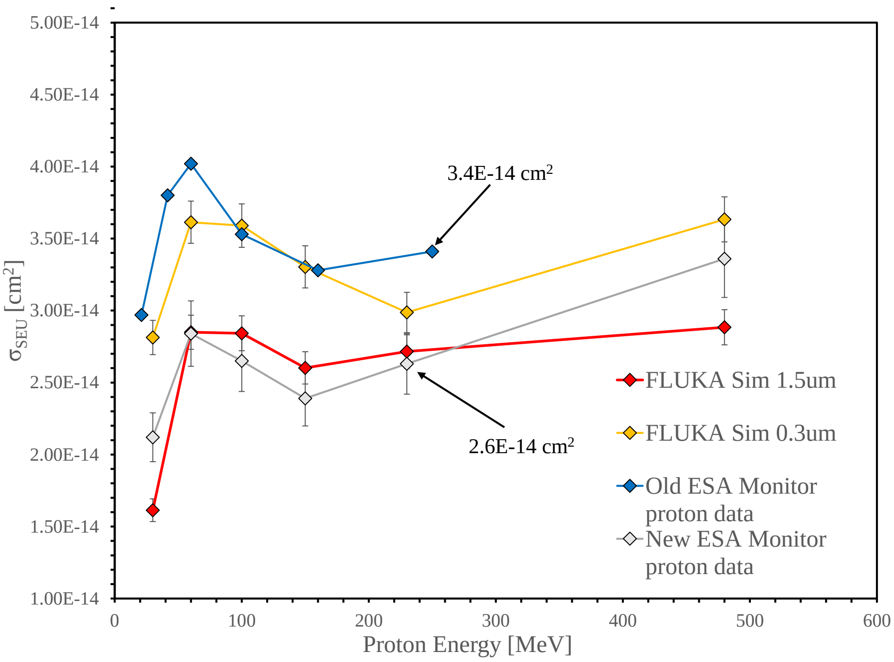

FIGURE 6.2: Simulated SEU cross-sections for protons as a function of their energy. The blue points correspond to measurements made with the old ESA SEU monitor and the grey the new monitor. As expected based on fig. 6.1, a 0.3 μm thickness reproduces the old data while a 1.5 μm thickness reproduces the new data.

We can clearly see that using a sensitive volume thickness of 0.3 μm reproduces the experimental data taken with the old monitor to high accuracy. Furthermore, our results using a 1.5 μm thickness are consistent with measurements made using the new monitor. Note that the calibration of our response function was entirely independent of experimental proton data. Simply using heavy ion measurements to feed into our fit was enough to reproduce proton results to high accuracy.

6.2 Simulating the Above Threshold Region

Now that we have determined a sensitive volume thickness to use in our simulations and have built a response function (which is dependent on the sensitive volume thickness) to weight energy deposition events, we can simulate heavy ion SEU cross-sections in the region above the LET threshold. In particular we look at the region above the knee with an LET of 4.5 MeVcm^2 /mg or greater. The results are shown in fig. 6.3.

The simulation matches the experimental data extremely well but note that this is by construction. We built our response function such that when it is applied to our data this

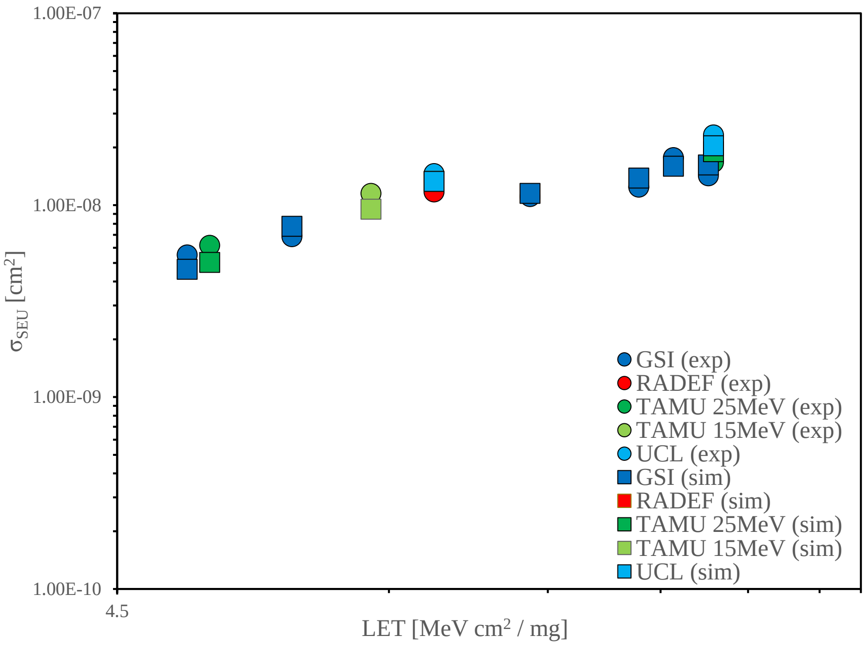

FIGURE 6.3: The simulated and experimental data points for the various facilities shown for incident ions with an LET > 4.5 MeV cm^2/mg

above threshold region would be reproduced. Thus, the results here come out naturally from our calibration.

6.3 Simulating the Sub-Threshold Region

Next we ran our simulations for the heavy ions that are in the region clearly below the knee and subsequently only produce SEUs through the generation of secondary particles through nuclear interactions. The results are shown in fig. 6.4. We can immediately see that the results here do not match the experimental data well. This is to be expected considering the fact that this region is very sensitive to our geometric variables.

The discrepancies between the simulated and experimental cross-sections appear to be dependent on the energy of the incident ion. This can more clearly be seen in fig. 6.5 and in table table 6.1. While the physics behind the FLUKA simulation suggests a decreasing σ_{SEU} with energy per nuclei of the primary ion, the experimental results suggest otherwise. This is just a manifestation of what was shown in fig. 2.4. The result is that our simulated GSI points are a factor ~3 lower than experiment, RADEF & UCL points a factor of ~10 lower, and the TAMU point a factor ~300 lower.

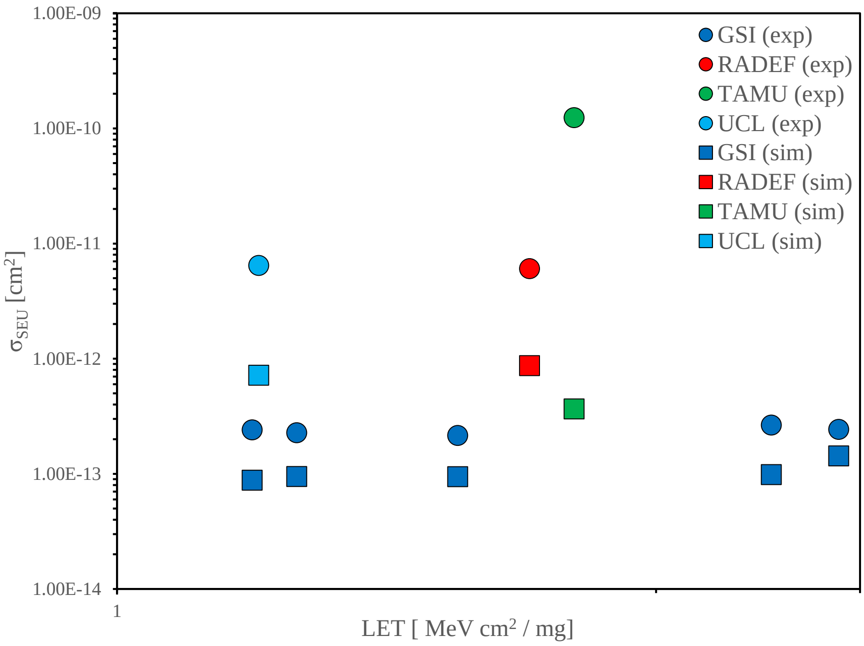

FIGURE 6.4: The simulated and experimental data points for the various facilities shown for incident ions with an LET < 2.6 MeV cm^2/mg.

Facility	Energy [MeV/u]	σ_{exp} [$\times 10^{-13}$cm^2]	σ_{sim} [$\times 10^{-13}$cm^2]	$\sigma_{exp}/\sigma_{sim}$
RADEF	9.3	60.4	8.70	7.0
UCL	10.1	64.4	7.17	9.0
TAMU	25	1240	3.66	340
GSI	193	2.43	1.43	1.7
GSI	290	2.65	0.98	2.7
GSI	496	2.15	0.94	2.3
GSI	996	2.27	0.95	2.4
GSI	1497	2.41	0.88	2.7

TABLE 6.1: Discrepancy between simulated and experimental cross-sections as a function of primary ion energy for incident ions with an LET < 2.6 MeV cm^2/mg

We now investigate how varying our geometric variables within accessible phase space impacts our SEU cross-sections in the sub-threshold region.

6.3.1 Sensitive Volume Thickness

From our proton simulations in fig. 6.1 we determined that a sensitive volume thickness of 0.5 μm should be reasonably representative of our effective volume. However, in the

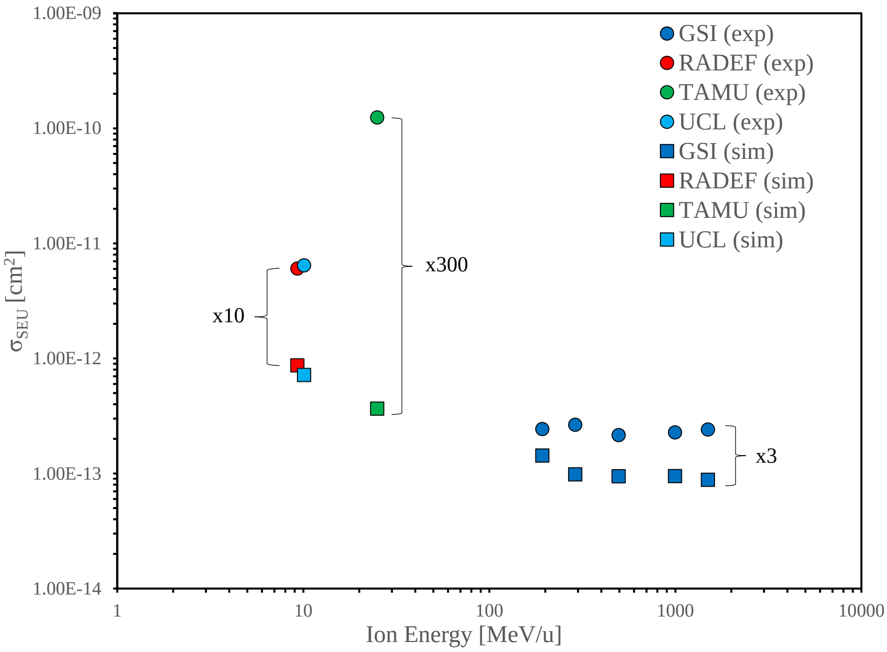

FIGURE 6.5: Simulated and experimental data points for the various facilities shown as a function of primary ion energy for incident ions with an LET < 2.6 MeV cm^2/mg

sub-threshold region where nuclear interactions dominate, the SEU cross-sections of the incident heavy ions could potentially have a strong dependence on this sensitive volume and so we perform simulations to test this. We ran our simulations for two ions in the sub threshold region: 56Fe at 996 MeV/u and 13C at 10.1 MeV/u. This gives us a high and low energy ion to test on to see if there is a potential energy dependence. The results are shown in fig. 6.6.

We see that there is very little if any dependence of σ_{SEU} on the sensitive volume thickness. This was to be expected since we already saw that there was a weak dependence in the case of protons which also induce SEUs via nuclear interactions.

6.3.2 Back End of Line

Next we investigate the impact of a thicker BEOL. As discussed in chapter 4, the BEOL is a set of SiO_2 and Al layers that are placed in front of the sensitive volume in the ESA SEU monitor. The thickness of this layer is particularly important for sub-threshold heavy ions as it provides an additional material through which nuclear interactions can occur, creating additional, higher LET ions that can go on to cause SEUs in the device. We investigate BEOL thicknesses of 6.7 μm (the expected physical thickness), 10 μm,

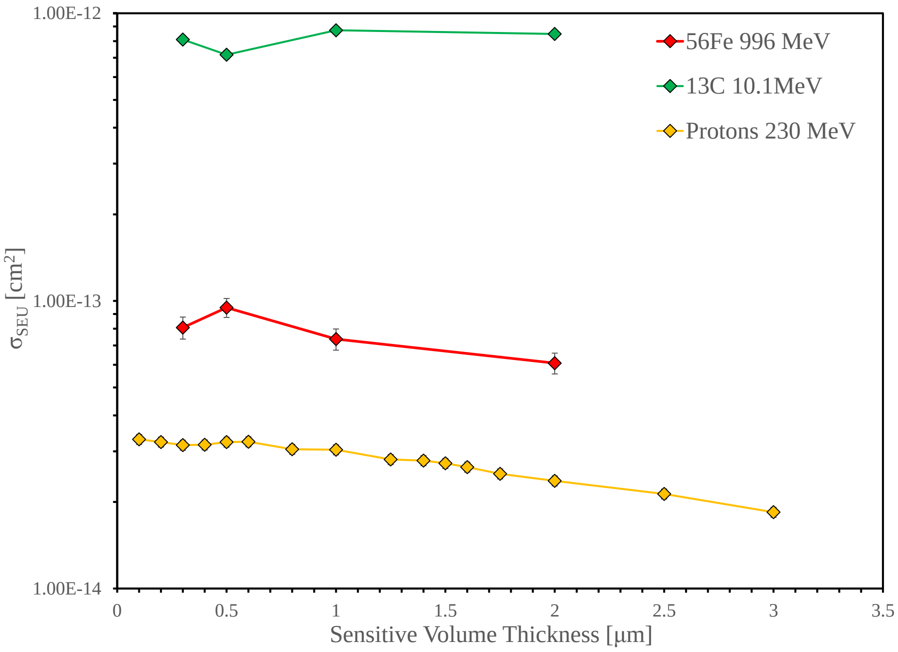

FIGURE 6.6: SEU cross-section dependence on sensitive volume thickness is shown for two ions in the sub-threshold region.

and 20 μm. Anything larger is not realistic. The simulations are performed for a sample of heavy ions in the sub-threshold region and the results are shown in fig. 6.7.

Clearly, the BEOL does not seem to impact the SEU cross-section for high energy protons and ions but it does have an impact on lower energy ions such as those at TAMU and RADEF. Extending the BEOL thickness from 6.7 μm to 20 μm increases the SEU cross-section of these ions by about a factor of 2. The source of this increase can be seen more clearly by looking at figs. 6.8 and 6.9. In the case of 13C at 10.1 MeV/u, we see additional events occurring at large energies above $\sim$ 200 keV. These events are caused by nuclear interactions and have a non-zero probability of inducing an SEU and so the SEU cross-section increases. However, for the case of 56Fe at 996 MeV/u, we see very little difference in the number of events in this high energy region despite an increase in the BEOL thickness and so the SEU cross-section remains the same.

6.3.3 Substrate

In addition to investigating the impact of a thicker BEOL in front of the sensitive volume, we investigate the impact of a thicker substrate behind the sensitive volume. Intuitively we would expect a very weak dependence at most of the SEU cross-section on

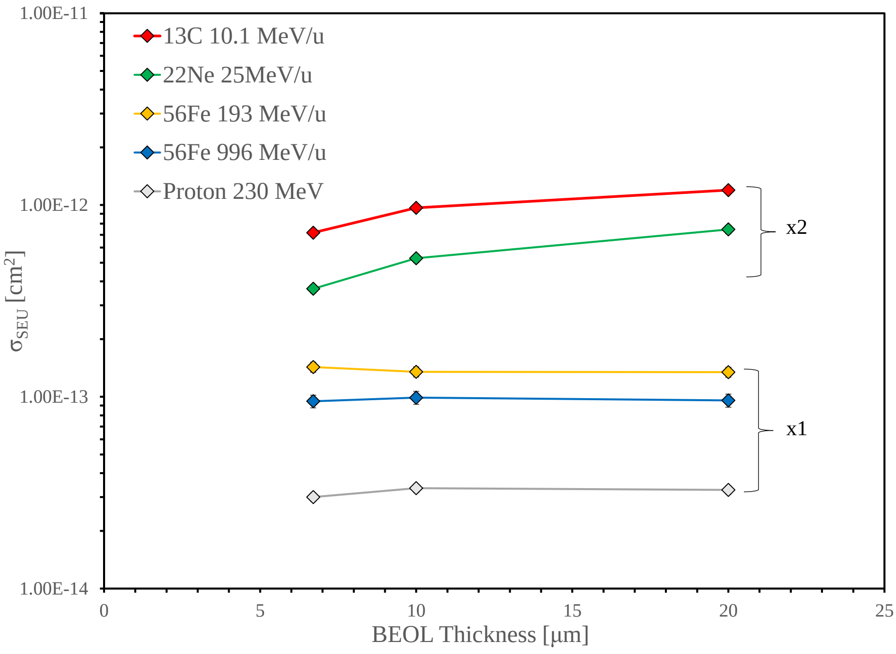

FIGURE 6.7: σ_{SEU} for high energy heavy ions and protons appears to be independent of the BEOL thickness whereas low energy heavy ions can have their σ_{SEU} increase by a factor of 2 by increasing the BEOL thickness.

the substrate thickness. It would be very surprising if a significant fraction of secondaries produced in this layer would backscatter and cause SEUs in the device. Nevertheless, for the purpose of performing an exhaustive analysis we perform simulations for 56Fe at 996 MeV/u and 13C at 10.1 MeV/u at substrate thicknesses of 2.3 μm, 20 μm, and 50 μm. The results are shown in fig. 6.10.

We see that for both protons and high energy iron ions, the SEU cross-section is statistically independent of the substrate thickness. Surprisingly, for low energy carbon ions there is a very small dependence on the thickness, suggesting that there is a fraction of secondaries backscattering and inducing SEUs in the device. However, this increase is only $\sim$20% when the thickness is increased from 2.3 μm to 50 μm and can not explain the discrepancies shown in fig. 6.5.

6.3.4 Side Effects

A limitation of our simulation is that we can only simulate a fraction of the sensitive volumes in the 4 Mbit ESA SEU monitor. For all of the simulated data shown thus far, we have used 16 sensitive volumes in our geometry. We now investigate the impact

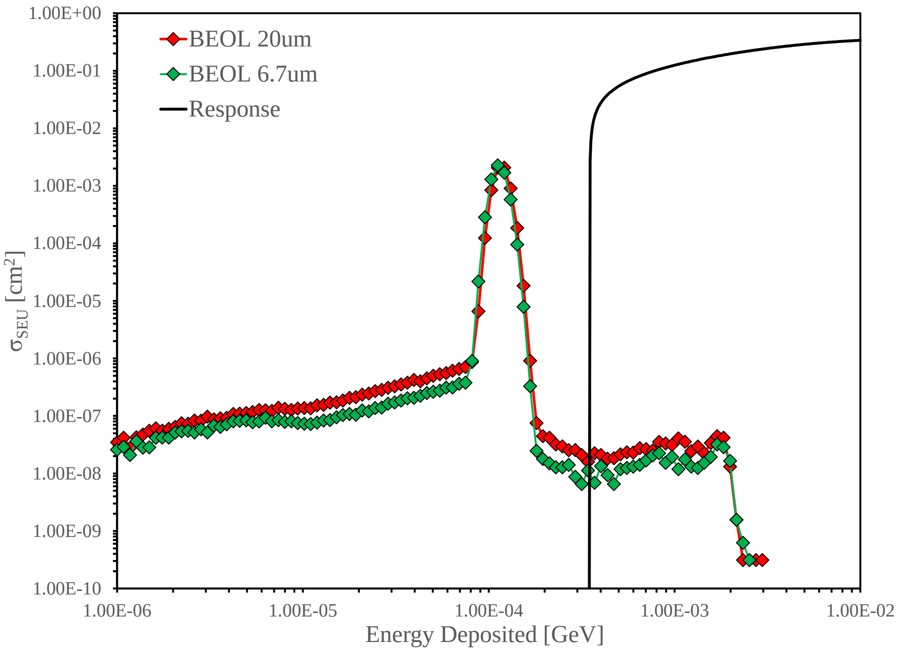

FIGURE 6.8: Energy deposition spectrum of 13C @ 10.1 MeV/u width varying BEOL thickness.

that this cut in the physical geometry has on our simulated SEU cross-sections. We parametrize the cut in terms of the beam size where for 1 SV, a beam size of 5×5 μm is used. For 16 SVs, a beam size of 40×40 μm is used. Finally, for 400 SVs, a beam size of 200×200 μm is used. There is always some margin between the lateral size of the implemented SRAM geometry and the beam size implemented. We perform simulations for a handful of ions in the sub-threshold region with different energies to see if there is an energy dependence. The results are shown in fig. 6.11 and tabulated in table 6.2

The results are exactly what we would expect. When there is only 1 sensitive volume simulated, nuclear reactions that produce a secondary that is directed at an angle away from the incident beam may miss the only sensitive volume and register no SEU in the simulation. In reality there would be adjacent SVs that could be encountered by this secondary. If we include 16 sensitive volumes and a larger beam, the systematic bias in our results induced by these secondaries is severely diminished since there are now additional sensitive volumes for the secondaries to cause bit flips in. Further increasing the number of sensitive volumes to 400 would reduce the impact even more, however, we see in fig. 6.11 that σ_{SEU} saturates at roughly 16 SVs. Thus, the simulations we have performed using 16 SVs appear to be accurate enough to account for side effects.

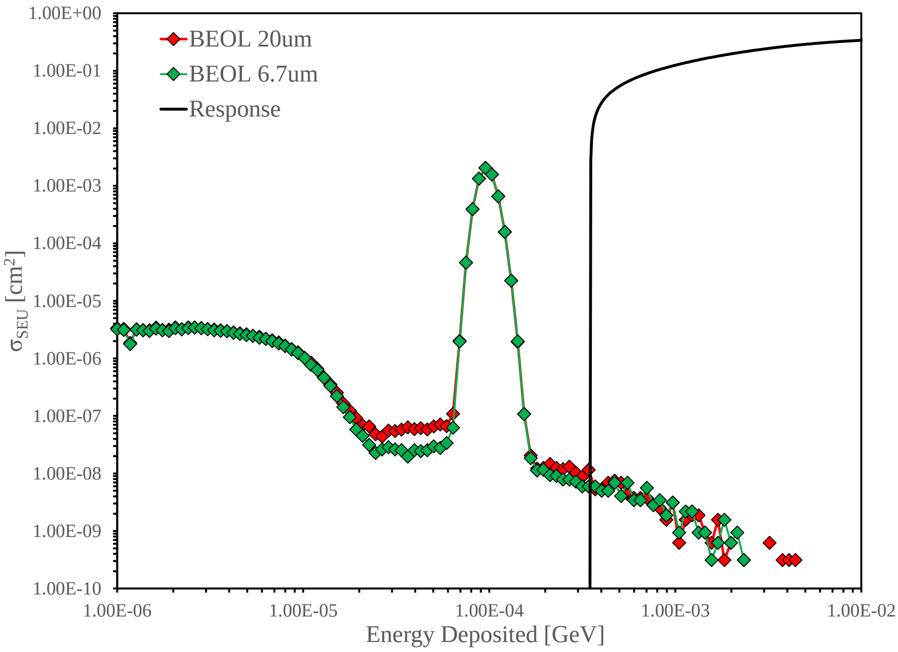

FIGURE 6.9: Energy deposition spectrum of 56Fe @ 996 MeV/u width varying BEOL thickness.

Ion	Energy [MeV/u]	# of SVs	σ_{SEU} [$\times 10^{-13}$cm^2]	Ratio to 16 SVs
13C	10.1	1	3.52 ± 0.08	0.26 ± 0.03
13C	10.1	16	7.2 ± 0.2	1.0 ± 0.1
13C	10.1	400	7.3 ± 0.2	1.1 ± 0.1
22Ne	25	1	1.34 ± 0.05	0.37 ± 0.02
22Ne	25	16	3.7 ± 0.2	1.00 ± 0.06
22Ne	25	400	4.0 ± 0.2	1.10 ± 0.07
56Fe	193	1	0.39 ± 0.02	0.28 ± 0.02
56Fe	193	16	1.43 ± 0.09	1.00 ± 0.09
56Fe	193	400	1.29 ± 0.08	0.90 ± 0.08
56Fe	996	1	0.25 ± 0.02	0.26 ± 0.03
56Fe	996	16	0.95 ± 0.07	1.0 ± 0.1
56Fe	996	400	1.01 ± 0.07	1.1 ± 0.1
Proton	230	1	0.109 ± 0.004	0.34 ± 0.02
Proton	230	16	0.32 ± 0.01	1.00 ± 0.06
Proton	230	400	0.33 ± 0.01	1.02 ± 0.06

TABLE 6.2: Simulated SEU cross-section as a function of the number of sensitive volumes simulated.

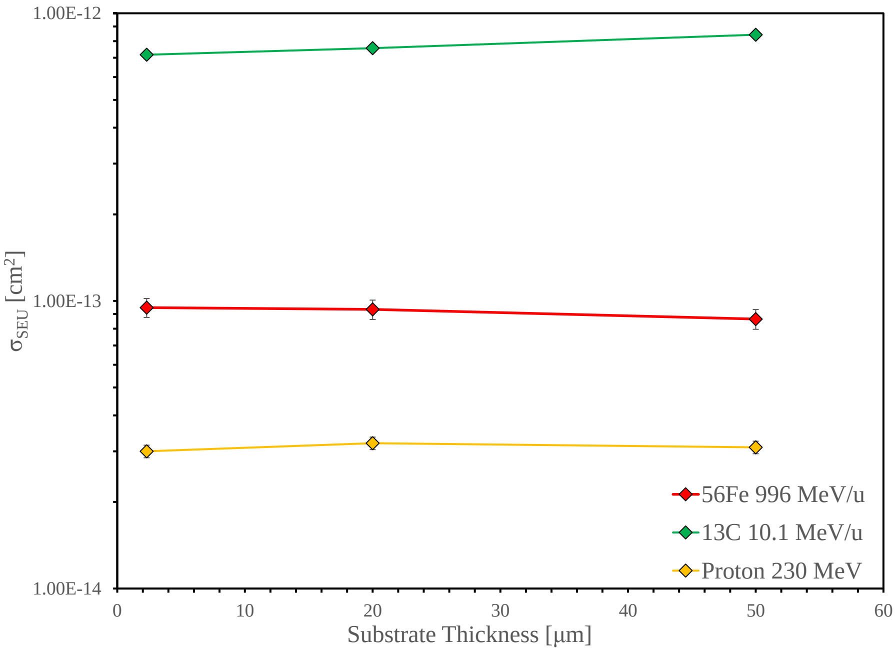

FIGURE 6.10: SEU cross-sections for a high and low energy ion in the sub-threshold region are shown as a function of substrate thickness.

6.3.5 Air

As mentioned in chapter 4, TAMU and GSI do not perform their SEU measurements in a vacuum. Instead they have 2 cm and 1 m of air, respectively, in-between the beam and the DUT. Furthermore, measurements were taken at RADEF for 15N @ 9.3 MeV/u both in a vacuum and with 1 cm and 3 cm of air in-between the beam and the DUT. A four-fold increase was observed in the SEU cross-section from vacuum to 1 cm of air at RADEF [18].

In practice, reproducing this air in simulations is difficult to do. The reason for this is because the thickness of the air is very large with respect to the dimensions of the electronics in question. When the beam interacts with the air, secondaries and primaries will scatter and by the time they reach the DUT they can be displaced by several cm from the initial beam direction. This means that in order to “catch” these ions with the ESA monitor, we would need to simulate a very large section of the 4Mbit SRAM (on the order of the thickness of air simulated). This is not feasible due to computational limitations.

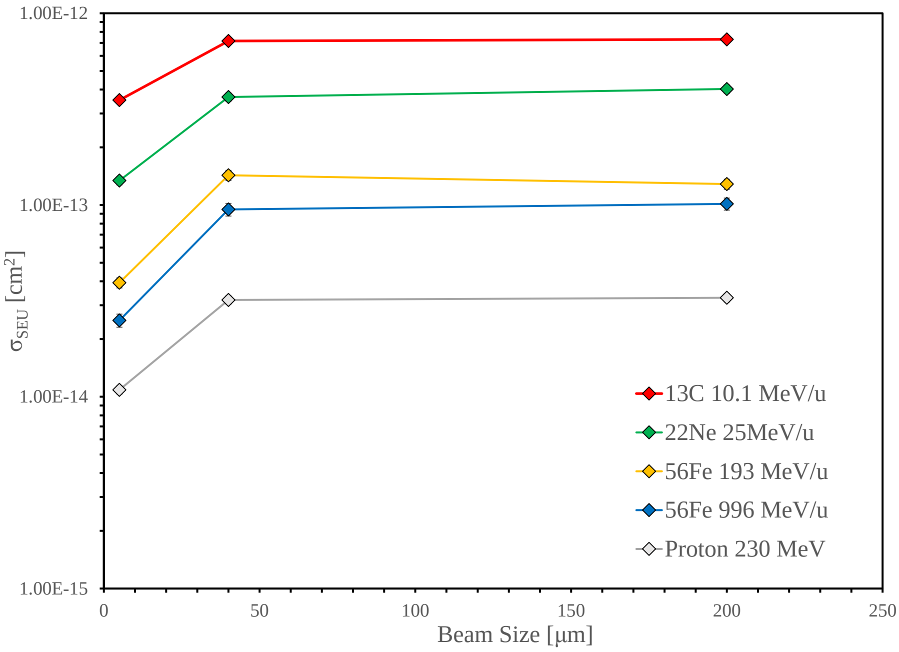

FIGURE 6.11: The SEU cross-section for low LET heavy ions is shown for varying beam sizes corresponding to the simulation of an increasing number of sensitive volumes. The beam size quoted is the side size of a square beam.

Instead, our approach is to simply perform a simulation of a large surface area of BEOL through which the particles can interact after passing through the air. We perform our simulations in FLUKA without any other components of the monitor implemented in the geometry and we simply score the LET of all particles that pass through the air and the BEOL. A sample resultant LET spectrum is shown in fig. 6.12. The distribution of ion species that reach this scoring region is shown in fig. 6.13.

We want to convolve this LET spectrum with a response function in order to arrive at an estimate for the SEU cross-section. In order to do this we first convert the LET spectrum in fig. 6.12 to the inverse cumulative distribution shown in fig. 6.14. This is a reverse integral of fig. 6.12 normalized to 1. To check the validity of our methodology thus far, we compare the resulting reverse integral to what we obtain from the energy deposition spectrum of a full simulation through the detector with no air implemented in the geometry. The energy deposition spectrum is converted to LET_{vol} and the reverse integral is shown in fig. 6.15 for comparison. We see that up to an LET of ~ 10 MeV cm^2/mg the two distributions are in strong agreement. After this point we see more high LET events occurring in the full simulation. This is due to the fact that the volume-equivalent LET is reconstructed using the path length of travel through the

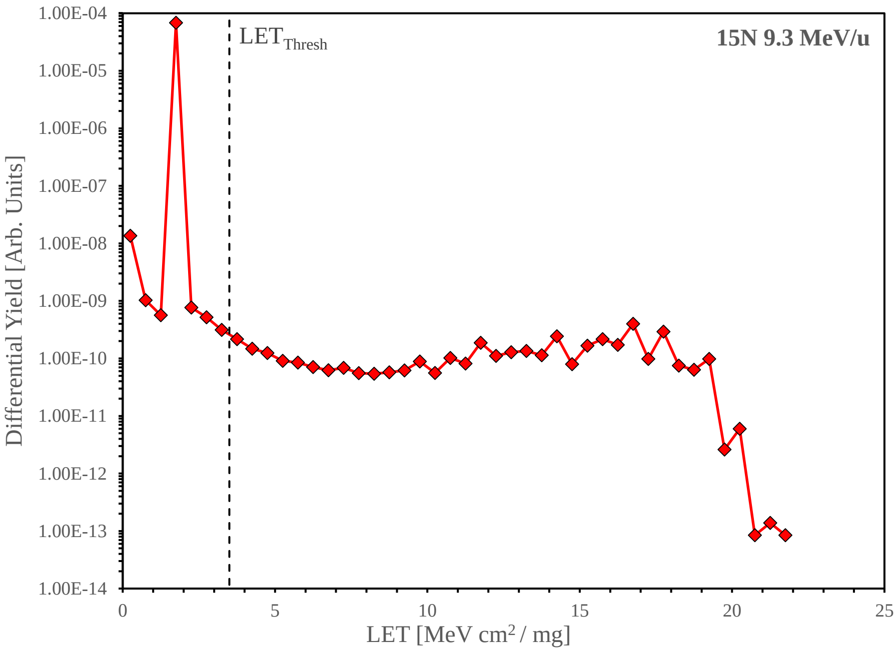

Figure 6.12: The LET Spectrum for 15N at 9.3 MeV/u is shown after the beam passes through 1 cm of air and 6.7 μm of BEOL. The approximate LET threshold is marked, below which ions do not have sufficient LET to cause upsets. We clearly see that ionization induced effects lie below this threshold and only nuclear interactions contribute to SEUs.

sensitive volume as outlined in eq. (2.2). In the full simulation the ions travel at angles through the sensitive volumes and therefore deposit more energy (over a longer path length). However, when we reconstruct the LET$_{\mathrm{vol}}$ we use the thickness of the sensitive volume which inflates the reverse integral in this region.

The spectrum we are dealing with is of the LET of the particles that passed through the BEOL. We cannot use the same response function we've been using thus far because we no longer have a spectrum of reconstructed LET$_{\mathrm{vol}}$ after passing through a SV. Instead we need a response function that maps directly from LET to σ_{SEU}. This could be constructed by a maximum likelihood Weibull fit on the experimental data above an LET of $\sim$ 3.0 MeV cm^2/mg. However, since we are only interested in the relative dependence of σ_{SEU} on the thickness of air between the ion source and the DUT, we only require relative accuracy. Thus, we can approximate our response function as a step function beginning at a threshold LET of $\sim$ 3.5 MeV cm^2/mg and saturating at $\sigma_{SAT} \simeq 2 \times 10^{-14}$ cm^2. The value of our inverse cumulative distribution at this LET multiplied by σ_{SAT} is then an estimate of our σ_{SEU} for the simulated geometry. This is

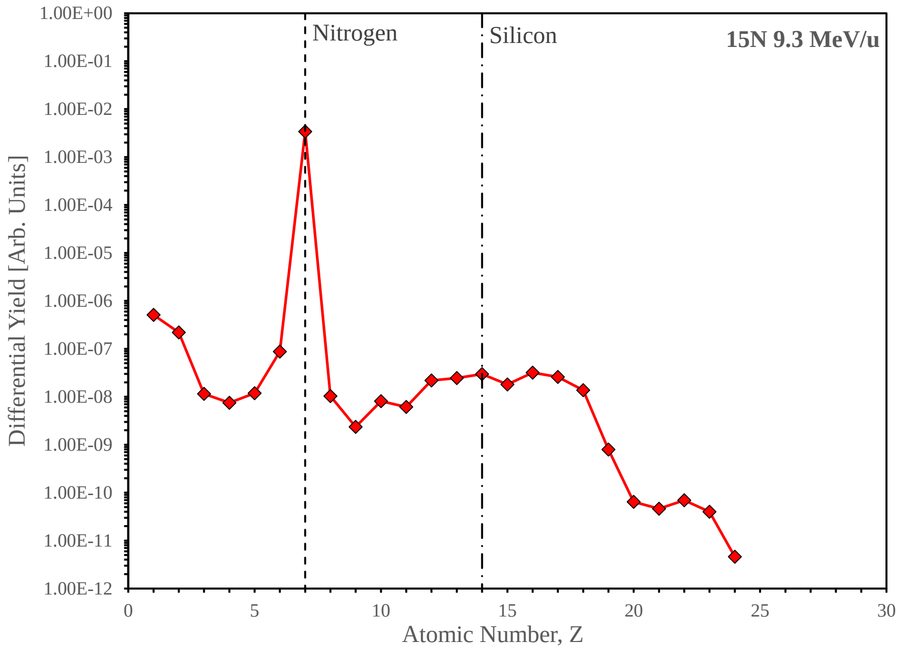

FIGURE 6.13: The distribution of ion species is shown after a beam of 15N at 9.3 MeV/u passes through 1 cm of air and 6.7 μm of BEOL.

perfectly acceptable for the purposes of determining the influence of air in front of the DUT in terms of the relative impact on the SEU cross-section.

As a cross-check, we again perform simulations using this methodology without any air. We simply perform LET scoring on 22Ne at 25 MeV/u using a 6.7 μm BEOL and a 20 μm BEOL to see if we can reproduce the results seen in fig. 6.7. We find that with 6.7 μm of BEOL $\sigma_{SEU} = 8.02 \times 10^{-13}\text{cm}^2$ whereas with 20 μm of BEOL $\sigma_{SEU} = 1.62 \times 10^{-12}\text{cm}^2$. This is precisely the factor of 2 increase that we see in fig. 6.7.

With the methodology motivated and validated, the results obtained through its implementation are shown for RADEF and TAMU in fig. 6.16 for simulated thicknesses of air of 0, 1, 2, 3, and 10 cm.

We can see that our simulated results for RADEF do not show the factor of four increase observed experimentally when going from vacuum to 1 cm of air. Instead we only see a 20% increase in the SEU cross-section for this transition and an 80% increase going to 10 cm of air. This suggests that perhaps it is the air/vacuum transition foil that dominates the experimentally observed increase in σ_{SEU} as opposed to the air itself. Furthermore, we see that for the TAMU ion, statistically there is absolutely no impact of introducing air into the environment. Again, in reality the air/vacuum transition foil

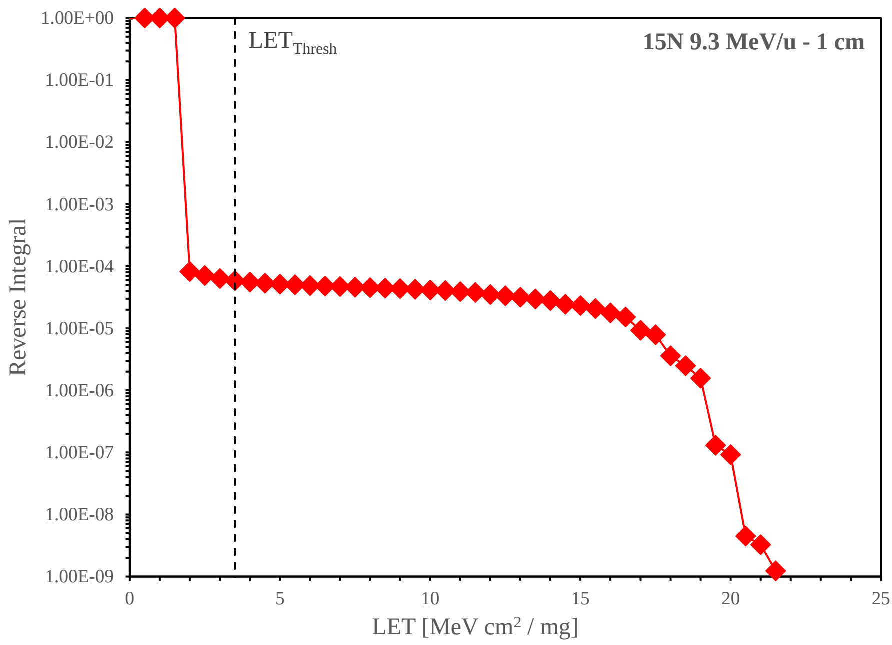

FIGURE 6.14: The reverse integral for 15N @ 9.3 MeV/u is shown after the beam passes through 1 cm of air and 6.7 μm of BEOL. The value of this function at $\text{LET}_{\text{Thresh}}$ of $\sim$ 3.5 MeV cm^2/mg multiplied by σ_{SAT} gives an estimate of σ_{SEU} for this air thickness.

could play a role but as this is typically only ∼10 μm of stainless steel, it is hard to justify an appreciable increase in σ_{SEU}.

6.4 IRPP vs. Nested Volume

Finally, we investigate the compatibility of the results obtained using the IRPP model presented herein and the Nested Volume approach applied to the same data explored in [24]. The simulated SEU cross-sections for a sample of low LET ions are given in table 6.3. We see that the IRPP model results in cross sections that are ∼20% larger at low energies and ∼200% larger at high energies. However, due to the computationally intensive nature of the Nested Volume approach, the Nested Volume cross-sections quoted result from the simulation of only a single sensitive volume whereas the IRPP cross-sections come from the simulation of 16 sensitive volumes. Considering the results shown in fig. 6.11 and table 6.2 it appears that the models are in strong agreement at high energies and the IRPP model results in slightly smaller cross-sections at low energies.

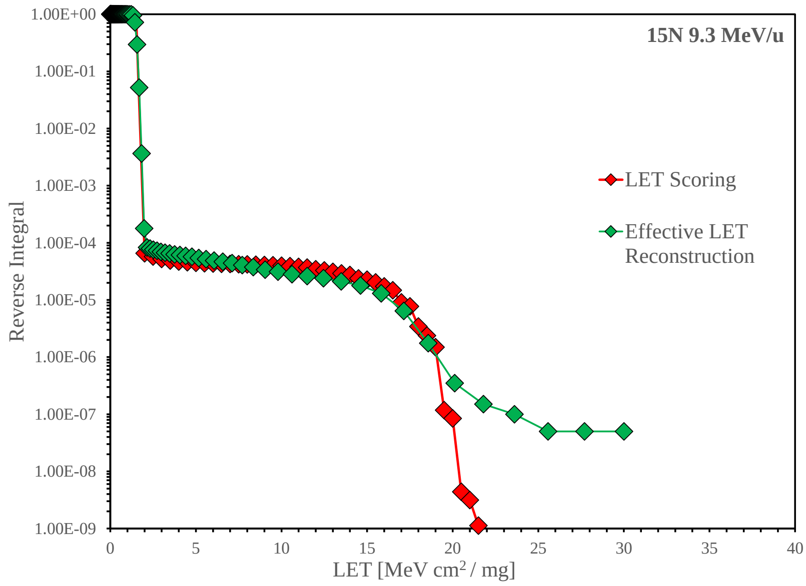

FIGURE 6.15: Inverse cumulative distributions obtained by scoring the LET after passing through solely 6.7μm of BEOL and by reconstructing $\mathrm{LET}_{\mathrm{eff}}$ after a full simulation through the detector.

Ion	Energy [MeV/u]	IRPP σ_{SEU} [$\times 10^{-13}$ cm^2]	Nested Volume σ_{SEU} [$\times 10^{-13}$ cm^2]	IRPP / Nested Volume
15N	9.3	8.7 ± 0.3	8.0 ± 1.0	1.1 ± 0.1
13C	10.1	7.2 ± 0.2	6.0 ± 1.0	1.2 ± 0.2
22Ne	25	3.7 ± 0.2	2.9 ± 0.2	1.3 ± 0.1
56Fe	496	0.94 ± 0.07	0.40 ± 0.08	2.4 ± 0.5
56Fe	1497	0.95 ± 0.07	0.32 ± 0.07	3.0 ± 0.7

TABLE 6.3: σ_{SEU} obtained by the IRPP approach is compared to those obtained using the Nested Volume model.

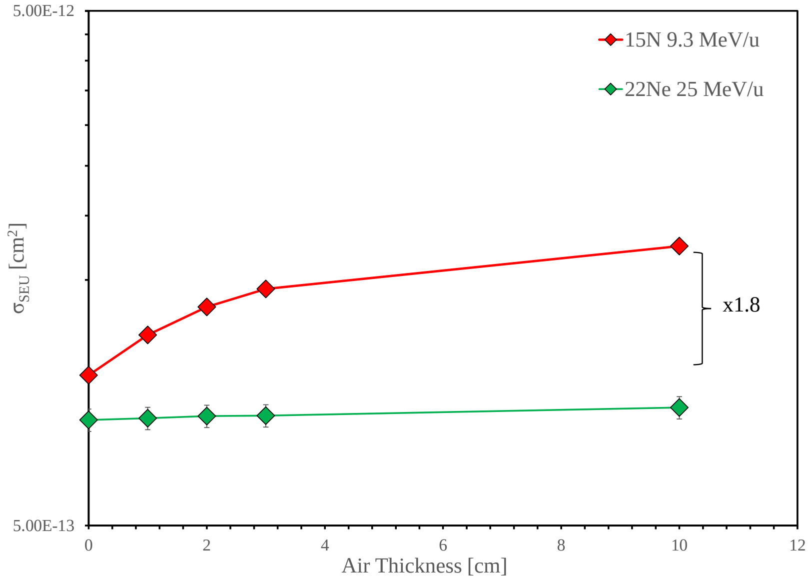

FIGURE 6.16: The simulated SEU cross-sections for varying thicknesses of air are shown for both 15N at 9.3 MeV/u and 22Ne at 25 MeV/u.

Chapter 7

Discussion and Conclusion

This study analyzed a large sample of experimental measurements made of heavy ion induced single event upsets in the ESA SEU monitor. An IRPP model was implemented through the use of FLUKA that was calibrated using measurements made of SEU cross-sections above the LET threshold. This model was successful in reproducing proton induced SEU data that was completely independent of our calibration. However, in the sub-threshold region the model underestimates the SEU cross-sections by a factor of $\sim$3 for the high energy ions at GSI, a factor of $\sim$10 for the ions at UCL/RADEF, and an anomalous factor of $\sim$300 for the ion at TAMU.

Several possible sources of systematic underestimation have been investigated. First, it has been shown that the model is independent of the thickness of the sensitive volumes. It was also observed that an increase in the BEOL of thickness from 6.7 μm to 20 μm results in a 200% increase in the SEU cross-sections for the low energy ions at UCL, RADEF, and TAMU. Furthermore, increasing the thickness of the substrate has been shown to have a negligible impact on the results and that the simulation of 16 SVs is enough to accurately take into account side effects. Finally, it was shown that including air in the simulations does not appreciable change the SEU cross-sections.

Clearly, more investigation is needed in order to understand the anomalous SEU cross-section measured at TAMU as the results show that this measurement is not physically motivated. It would be interesting to extend the data-sets considered in this study to components with larger LET thresholds. This would provide much more data in the sub-threshold region and allow for more in-depth analysis of energy and species dependencies. Furthermore, when possible, independent measurements should be made of SEU cross-sections for low LET ions in the same 25 MeV/u energy range explored by TAMU.

7.1 Acknowledgements

I would like to extend my sincere gratitude to Rubén Garcia Alia who devoted a great deal of time patiently explaining the very basic to the most detailed concepts relevant to this study. Thank you to Markus Brugger for helpful comments and to NSERC for an Undergraduate Student Research Award as well as IPP and CERN for an IPP CERN Summer Student Fellowship.

Bibliography

[1] "Radiation to electronics." http://r2e.web.cern.ch/R2E/. Accessed: 2014-08-15.

[2] K. Røed, M. Brugger, D. Kramer, P. Peronnard, C. Pignard, G. Spiezia, and A. Thornton, "Method for measuring mixed field radiation levels relevant for sees at the lhc," *Nuclear Science, IEEE Transactions on*, vol. 59, no. 4, pp. 1040–1047, 2012.

[3] K. Roed, V. Boccone, M. Brugger, A. Ferrari, D. Kramer, E. Lebbos, R. Losito, A. Mereghetti, G. Spiezia, and R. Versaci, "Fluka simulations for see studies of critical lhc underground areas," *Nuclear Science, IEEE Transactions on*, vol. 58, no. 3, pp. 932–938, 2011.

[4] R. Harboe-Sorensen, F.-X. Guerre, and A. Roseng, "Design, testing and calibration of a" reference seu monitor" system," in *Radiation and Its Effects on Components and Systems, 2005. RADECS 2005. 8th European Conference on*, pp. B3–1, IEEE, 2005.

[5] R. Harboe-Sorensen, C. Poivey, F.-X. Guerre, A. Roseng, F. Lochon, G. Berger, W. Hajdas, A. Virtanen, H. Kettunen, and S. Duzellier, "From the reference seu monitor to the technology demonstration module on-board proba-ii," *Nuclear Science, IEEE Transactions on*, vol. 55, no. 6, pp. 3082–3087, 2008.

[6] R. Harboe-Sorensen, C. Poivey, N. Fleurinck, K. Puimege, A. Zadeh, F.-X. Guerre, F. Lochon, M. Kaddour, L. Li, D. Walter, *et al.*, "The technology demonstration module on-board proba-ii," *Nuclear Science, IEEE Transactions on*, vol. 58, no. 3, pp. 1001–1007, 2011.

[7] R. Harboe-Sorensen, C. Poivey, A. Zadeh, A. Keating, N. Fleurinck, K. Puimege, F.-X. Guerre, F. Lochon, M. Kaddour, L. Li, *et al.*, "Proba-ii technology demonstration module in-flight data analysis," *Nuclear Science, IEEE Transactions on*, vol. 59, no. 4, pp. 1086–1091, 2012.

[8] E. Petersen, *Single event effects in aerospace.* John Wiley & Sons, 2011.

[9] G. K. Steinberg, J. I. Fabrikant, M. P. Marks, R. P. Levy, K. A. Frankel, M. H. Phillips, L. M. Shuer, and G. D. Silverberg, "Stereotactic heavy-charged-particle bragg-peak radiation for intracranial arteriovenous malformations," *New England Journal of Medicine*, vol. 323, no. 2, pp. 96–101, 1990.

[10] P. Dodd, J. Schwank, M. Shaneyfelt, J. Felix, P. Paillet, V. Ferlet-Cavrois, J. Baggio, R. Reed, K. Warren, R. Weller, *et al.*, "Impact of heavy ion energy and nuclear interactions on single-event upset and latchup in integrated circuits," *Nuclear Science, IEEE Transactions on*, vol. 54, no. 6, pp. 2303–2311, 2007.

[11] R. Reed, R. Weller, M. Mendenhall, J. Lauenstein, K. Warren, J. Pellish, R. Schrimpf, B. Sierawski, L. Massengill, P. Dodd, *et al.*, "Impact of ion energy and species on single event effects analysis," *IEEE Transactions on Nuclear Science*, vol. 54, no. 6, pp. 2312–2321, 2007.

[12] E. Petersen, "Cross section measurements and upset rate calculations," *Nuclear Science, IEEE Transactions on*, vol. 43, no. 6, pp. 2805–2813, 1996.

[13] S. K. Hoffgen and S. Metzger, "Investigation and analysis of very high energy accelerators for radiation simulation," *Fraunhofer INT*, vol. 323, no. 2, pp. 96–101, 2011.

[14] GSI Helmholtz Centre for Heavy Ion Research. Darmstadt, Germany [Online]. Available: http://www.gsi.de/portrait/index_e.html.

[15] UCL Cyclotron Resource Centre. Louvain-la-Neuve, Belgium [Online]. Available: http://www.cyc.ucl.ac.be/index.php.

[16] Radiation effects facility. Jyväskylä, Finland [Online]. Available: https://www.jyu.fi/fysiikka/en/research/accelerator/radef.

[17] Radiation effects facility. College Station, Texas, Texas A&M Univ. [Online]. Available: http://cyclotron.tamu.edu/ref/.

[18] V. Ferlet-Cavrois, J. R. Schwank, S. Liu, M. Muschitiello, T. Beutier, A. Javanainen, A. Hedlund, C. Poivey, A. Mohammadzadeh, R. Harboe-Sorensen, *et al.*, "Influence of beam conditions and energy for see testing," *Nuclear Science, IEEE Transactions on*, vol. 59, no. 4, pp. 1149–1160, 2012.

[19] "Fluka." http://www.fluka.org. Accessed: 2014-07-02.

[20] B. D. Sierawski, J. A. Pellish, R. A. Reed, R. D. Schrimpf, K. M. Warren, R. A. Weller, M. H. Mendenhall, J. D. Black, A. D. Tipton, M. A. Xapsos, *et al.*, "Impact of low-energy proton induced upsets on test methods and rate predictions," *Nuclear Science, IEEE Transactions on*, vol. 56, no. 6, pp. 3085–3092, 2009.

[21] C. Inguimbert, S. Duzellier, T. Nuns, and F. Bezerra, "Using subthreshold heavy ion upset cross section to calculate proton sensitivity," *Nuclear Science, IEEE Transactions on*, vol. 54, no. 6, pp. 2394–2399, 2007.

[22] P. Walden, "Relating delta ray energy to beam energy." TRIUMF.

[23] R. Ladbury, "Statistical properties of see rate calculation in the limits of large and small event counts," *Nuclear Science, IEEE Transactions on*, vol. 54, no. 6, pp. 2113–2119, 2007.

[24] C. Bahamonde, "Nuclear interaction contribution to seus in heavy ion energy deposition in the esa monitor," 2013. Available on CDS.